RECOMMENDING SAFE BICYCLE ROUTES

KAMONPHAN PHANNITHIPRASERT

AN INDEPENDENT STUDY SUBMITTED IN PARTIAL FULFILLMENT OF THE

REQUIREMENT FOR THE DEGREE OF MASTER OF SCIENCE

IN DATA SCIENCE AND ANALYTICS

KMITL-DIGITAL ANALYTICS AND INTELLIGENCE CENTER, SCHOOL OF SCIENCE

KING MONGKUT'S INSTITUTE OF TECHNOLOGY LADKRABANG

2024

KMITL-2024-SC-M-017-027

Independent Study Title	Recommending safe bicycle routes
Student Name	Kamonphan Phannithiprasert
Student ID	65056004
Degree	Master of Science (Data Science and Analytics)
	KMITL-Digital Analytics and Intelligence Center
Year	2024
Independent Study Advisor	Assoc. Prof. Dr. Laor Boongasame

Abstract

Cycling as a regular means of transportation can assist Thailand in reaching its 2050 carbon neutrality target. However, concerns regarding the safety and attractiveness of cycling routes remain significant barriers to daily bicycle use among Bangkok residents. As a result, this study aims to develop a safe bike route recommendation system that takes into account both the safety and attractiveness of cycling routes. The study utilizes diverse open-source data, including points of interest (POI), bike networks, and street view images, to extract indicators that influence cyclists' route choices. The study's conclusions highlight the value of bicycle route guiding systems. This approach allows users to ride more comfortably on regular days by avoiding traffic jams and other obstacles. Also, the recommended path only gained 5% more distance than the shortest one—a distance that cyclists typically ride within reasonable bounds.

Keywords : Safe Route Recommendation, Carbon Neutrality, Bikeability Indicator

Acknowledgments

I would like to extend my sincere appreciation to Assoc. Prof. Dr. Laor Boongasame for her invaluable guidance, encouragement, and support throughout this project. Her expertise and insights have helped to shape the direction of this study.

I am also grateful to my classmates, whos generously shared their time and information; without them, this study would not have been possible.

Furthermore, I would like to acknowledge the support and understanding of my family and friends, whose encouragement has been a constant source of motivation.

Lastly, I am thankful to the authors, whose research and insights have provided inspiration and knowledge for this study.

Kamonphan Phannithiprasert

List of Contents

List of Contents (Cont.)

Page

List of Contents (Cont.)

Page

List of Tables

List of Illustrations or Figures

Figure **Page**

List of Illustrations or Figures (Cont.)

Figure **Page**

Glossary

Term	Definition
Accessibility	An indicator reflecting the availability and proximity of amenities and services along a cycling route, such as shops, parks, and public facilities.
ADE20K	A dataset used for training semantic segmentation models, comprising both indoor and outdoor scenes.
Bikeability	the degree to which the actual and perceived environment is convenient and safe for bicycling. It is often based on indicators such as infrastructure, safety, accessibility, and visual environment.
Bikeability Map	A visual representation of an area's bikeability, highlighting routes and areas more suitable for cycling based on various indicators.
Bikeway Infrastructure	Physical structures and facilities specifically designed for bicycle use, such as bike lanes, bike paths, and bike racks.
Carbon Dioxide (CO_2)	A greenhouse gas produced by burning carbon-based fuels, respiration, and other processes, contributes significantly to global warming and climate change.
Cityscapes	A large-scale dataset contains images of urban street scenes. It is commonly used for training models in semantic segmentation and other computer vision tasks.
Crowdedness sub-Indicator	A measure used to assess the level of obstacles or number of people on a road reflected in visual perception indicator
Cycling Suitability	An indicator assessing the comfort and safety of a cycling route, taking into account factors like road curvature, lighting conditions, and the presence of bike lanes.
Cyclist-Centric Approach	A method of route planning that prioritizes the preferences, comfort, and safety of cyclists, rather than just focusing on distance or time efficiency.

Glossary (Cont.)

Term	Definition
Digital Elevation Model (DEM)	A 3D representation of a terrain's surface, typically used in geographic information systems for analysis of elevation and landform.
Geographic Information System (GIS)	A framework for gathering, managing, and analyzing spatial and geographic data.
Impedance	In the context of route planning, impedance refers to the resistance or cost associated with a particular route. Lower impedance indicates a more desirable route.
National Health Assembly (NHA)	A social mechanism that promotes evidence-based policymaking with a strong emphasis on inclusive participation, operating as a continuous, year-round process.
Nationally Determined Contribution (NDC)	A climate action plan to cut emissions and adapt to climate impacts, which each Party to the Paris Agreement is mandated to develop and revise a climate action plan every five years
OpenStreetMap (OSM)	A collaborative project to create a free editable map of the world. Recognized for its comprehensive road annotation and mapping, especially in urban areas.
Origin-Destination (OD) Pairs	Pairs of points are used to assess and compare different route options, typically representing the starting and ending points of a journey.
OSMnx Library	A Python package that simplifies the process of downloading, modeling, analyzing, and visualizing street networks from OpenStreetMap's data.
Point of Interest (POI)	Specific locations that someone may find useful or interesting, such as businesses, parks, schools, and landmarks.

Glossary (Cont.)

Term	Definition
Pre-Trained Model	A model learns from a large dataset initially to capture general patterns. Thus, it requires less data and computation for specific tasks
Semantic Segmentation	A process in computer vision that involves partitioning an image into multiple segments for analysis. Used in this study for classifying street view images.
Street View Image (SVI)	A panorama view of the street is retrieved from Google Maps Platform.
United Nations Framework Convention on Climate Change (UNFCCC)	An international treaty among countries for negotiating an agreement to limit the dangers of climate change.
Visual Perception	An indicator evaluating the visual surroundings experienced during cycling, including elements like scenery, street cleanliness, and visual interest.

Chapter 1
Introduction

Thailand, classified as a Non-Annex I Party under the United Nations Framework Convention on Climate Change (UNFCCC), is actively striving to achieve its long-term objectives of attaining carbon neutrality by 2050 and achieving net-zero greenhouse gas emissions by 2065. The development of the National Determined Contribution (NDC) Sectorial Action Plan for the Transport Sector, which spans from 2021 to 2030, places significant emphasis on efficient and sustainable transportation systems. One of the endorsed urban transportation methods that is both efficient and environmentally friendly is cycling (Office of Natural Resources and Environmental Policy and Planning, 2022). Selecting to cycle overtake a car once a day is an effective way to reduce carbon emissions per person by 67% on average (Hallisey, 2022). Furthermore, numerous studies have investigated the benefits of cycling. The findings indicate that cycling for 20 minutes daily can reduce the risk of mortality by at least 10%, decrease the likelihood of cardiovascular disease by 10%, lower the risk of type 2 diabetes by 30%, and decrease cancer-related mortality by 30% (World Health Organization, 2022).

Since 2012, Thailand has made investments in cycling infrastructure, establishing bicycle use as a policy. The new policy framework is known as the 2012 NHA resolution on “supportive systems and structures for walking and cycling in daily life” (National Health Commission Office, 2012). However, Ungsuchaval et al. (2022) recommend that the policy focus more on cultural meaning and cycling experience to promote cycling in everyday life. According to Bakker et al. (2018), factors such as (1) extensive detours, (2) dispersed bike lanes, (3) low safety, (4) minimal comfort, and (5) lack of appeal on larger roads hinder the adoption of cycling as a daily mode of transportation among Thai citizens.

Panthasen et al. (2021) suggest that the greatest potential for replacing motorized transport with non-motorized options is in short-distance trips, specifically those less than 3 kilometers. As a result, an effective approach would be to focus on improving safety, connectivity, and direct routes at the neighborhood level. Creating intelligent pedestrian and bicycle shortcuts between alleys can achieve this. This approach is more efficient

compared to the current strategy, which involves trying to establish extensive linear bicycle routes along already congested main roads.

Globally, people have embraced the use of bicycles as a sustainable urban transportation option for more than ten years (Anton-Gonzalez et al., 2023). The scientific community has populated various approaches to assess the bicycle-friendliness of the built environment, with "bikeability" being the most common (Codina et al., 2022). Castanon and Ribeiro (2021) systematize the data obtained from fourteen studies, leading to four core domains that characterize the bikeability concept:

1) Cycle infrastructure includes elements such as the presence of bicycle infrastructure, the presence of traffic lights and stop signs, the width of bike lanes, the presence of night lightning, and the condition of the surface.
2) Safety factors include the percentage of heavy wheels, the average speed of the road, the volume of traffic, and the separation of bicycle paths.
3) Accessibility factors, such as land use density or connectivity, are crucial.
4) Factors such as the slope of the road, the presence of natural elements, and the quality of the air.

Traditionally, on-site field observations, which are labor-intensive and cover limited areas, have determined bikeability indicators. While some studies use tools like Geographic Information Systems (GIS) to assess bikeability, they often miss street-level details seen by cyclists. Technological advancements now provide many images from pedestrian and cyclist perspectives. As a result, computer vision techniques such as semantic segmentation and object detection performed on street view images (SVI) are becoming popular in urban studies (Ito and Biljecki, 2021; Lin and Saxe, 2024).

Therefore, the study uses a framework that leverages open-source data, advanced deep learning techniques applied to street view images, and spatial analysis to achieve the following goals:

(1) **Bikeability Maps**: The study aims to create bikeability maps that evaluate various indicators to determine the suitability of different areas for cycling.
(2) **Safety Bike Route Recommendations for Daily Use**: The study aims to recommend the safest routes for daily use by considering factors such as

cyclists' visual perception, cycling infrastructure, and road length to prioritize the safety and attractiveness of the suggested routes.

In summary, this research utilizes data-driven methods and advanced technology to contribute to the improvement of sustainable urban transportation, public health, and urban planning in Thailand. It aims to enhance the cycling experience in urban areas by providing bikeability maps and safety bike route recommendations for daily use, starting with Khlong Toei district, Bangkok, Thailand.

Chapter 2 provides an overview of the research related to our objectives. Subsequently, Chapter 3 outlines the proposed framework, while Section 4 delves into the discussion of the study results. Lastly, Chapter 5 presents the comprehensive conclusions, limitations, and future research drawn from the study.

Chapter 2
Literature Reviews

2.1 Related Works

2.1.1 The Need for Cycling in Thailand

Human actions, primarily driven by the release of greenhouse gases, have led to global warming, resulting in a rise of 1.1°C above the 1850–1900 baseline during the period from 2011 to 2020. These contributions arise from unsustainable energy use, land use, and diverse lifestyles across regions, nations, and individuals (Intergovernmental Panel on Climate Change, 2023). Transportation in Thailand accounts for 27% of all greenhouse gas (GHG) emissions in the energy sector, similar to levels in the EU and the US. With the ambition of achieving net-zero GHG emissions by 2065 and carbon neutrality by 2050, one of the main GHG mitigation strategies focuses on the energy and transport sectors, including continued investment in zero-emission electric vehicles (EVs) (Office of Natural Resources and Environmental Policy and Planning, 2021). The European Cyclists' Federation (2011) estimates that if cycling rates in the 27 EU countries matched those in Denmark, bicycles could contribute 12 to 26% of the 2050 target reduction for the transportation sector. Thus, adopting this approach could be an effective strategy for supporting Thailand's GHG reduction mission.

2.1.2 Cycling Concerns in Thailand

Despite multi-year efforts by the Bangkok Metropolitan Administration (BMA) to promote cycling by improving 23 routes for cyclists, totaling 184.56 kilometers (Raha and Taweesin, 2013), CO2 emissions per person per year have not decreased (Ritchie et al., 2022). Cycling has mainly attracted recreational and fitness-oriented cyclists, but it has not gained substantial attention from those who use cycling as part of their daily routines (Ungsuchaval et al., 2022). This is partly due to the infrastructure, which is often constructed for sports and recreational purposes, such as routes around airports that are sometimes disconnected from the main transport network. Other cycling routes are

located on sidewalks and along main roads (Bakker et al., 2018). The lack of a noticeable increase in the number of utility cyclists indicates that the BMA has not successfully created conditions that meet Bangkok residents' needs. Five issues categorize the cycling situation in Thailand's urban areas.

1) Low safety: There are numerous crossings where bikes mix with motorized traffic, there aren't enough protected bike lanes, there aren't enough suitable bike paths, and there's a fear of crime.
2) Low directness: There are significant deviations from the starting point to the final destination and lengthy delays at traffic signals.
3) No coherence: Bike lanes are scattered, unconnected, and have different typologies.
4) Little comfort: Exposure to hazards, lack of shade, noise, and pollution are all present.
5) Attractiveness: It is good in quiet alleys and parks, but not attractive on bigger roads.

Safety concerns are the primary factor deterring residents of Bangkok from cycling, a result consistent with Thailand's ranking as the 9th highest country in terms of road traffic death rate, at 32.7 deaths per 100,000 population (World Health Organization, 2018; Bakker et al., 2018; Panthasen et al., 2020; World Health Organization, 2023).

2.1.3 Cycling Route Recommendation

Conventional planners primarily tailor their route recommendations for cars, public transport, and walking journeys, rarely considering cycling as a viable option. The primary objective of these conventional planners is to identify the shortest, quickest, or most cost-effective route (Ribeiro et al., 2022). However, there are limited options for cyclists in terms of driving navigation aids (Lau, 2020). Contrary to motorists, bikeability factors such as road surface quality, slopes, the number of necessary stops, and safety considerations significantly influence cyclists (Wage and Sester, 2021). Hardinghaus and Nieland (2021) categorized cyclists’s route preferences into four clusters: "Relax and Park," which involves calm roads and green pathways; "Comfort and Bike Path," which prioritizes smooth surfaces

and (partly) avoids main roads lacking cycle infrastructure; "Fast & Easy," which seeks main roads regardless of cycle infrastructure; and "Short," focusing on finding the shortest route. The authors concluded with a statement that “there is no ideal route and no ‘one-size-fits-all approach’, but rather distinct individual and trip-related preferences that determine route choices”. Therefore, finding routes that properly consider safety along with cyclists’ preferences tailored to daily use is essential to promoting cycling as a practical mode of transport.

To recommend safe bike routes for everyday transportation, there are two key steps to follow. First, compare the "bikeability" scores for different cycling routes, which are composed of the safety and other daily-use-preference indicator scores. Second, recommend a route with the highest score from origin to destination. The concept of bikeability originated from the idea of pedestrian walkability. Winters et al. (2013) introduced a bikeability framework in 2013; however, a widely accepted definition for "bikeability" is still lacking. According to Kellstedt et al. (2021), it is defined as the degree to which the actual and perceived environment is convenient and safe for bicycling. This has prompted researchers to develop various indicators to assess different aspects of the built environment that can influence cycling behavior. The presence of cycling infrastructure is a pivotal element in enhancing an area's bikeability, as cyclists strongly prefer facilities that separate them from motor traffic (Lin and Wei, 2018; Veillette et al., 2019). In addition to safety-related route attributes, cyclists also prioritize factors that enhance route comfort and the appeal of the surroundings, increasing the probability of choosing a safe route (Berghofer and Vollrath, 2023; Uijtdewilligen et al., 2023). To assess these surroundings, it is appropriate to use both street view images (SVI) and non-SVI approaches. Researchers commonly apply computer vision techniques like object detection and semantic segmentation (Mamidala et al., 2019; Ito and Biljecki, 2021; Tamagusko et al., 2023; Meng and Zheng, 2023). We thoroughly examine the five studies shown in Table 2.1 and 2.2. Two studies, Tamagusko et al. (2023) and Meng and Zheng (2023), not only constructed bikeability maps from bikeability scores but also recommended appropriate cycling routes based on those scores. Tamagusko et al. (2023) constructed a safety map and risk-aware routing system for micromobility users in Lisbon,

Portugal. The authors used object detection (YOLOv5) and image segmentation (NVIDIA) models to identify potential risk factors on cycling routes from 4-direction Google Street View Images (GSV). The authors built a safety map in collaboration with Bikeable, a unique neural network that predicts safety scores from images using a combination of object detection and semantic segmentation inputs. Meng and Zheng (2023) used multi-sourced data from both SVI and non-SVI sources, such as the Digital Elevation Model (DEM) and Point-of-Interest (POI), to calculate bikeability indicators in Namshan District, Shenzhen, China. They used DeepLabV3+ (a semantic segmentation model) to extract bikeability factors from 6-direction GSVs. The authors proposed routes by computing the impedance function from the bikeability scores.

Many studies in Thailand also use street view images. Mamidala et al. (2019) used SegNet (a semantic segmentation model) to detect street lanes in GSV. Tanprasert et al. (2020) also used U-Net, a semantic segmentation model, to recognize traffic black spots on street view images for safety issues. The researchers manually extract the Green View Index (GVI) from the GSV at Nakhon Ratchasima (Juntakut et al., 2022). On a Bangkok urbanscapes dataset, Thitisiriwech et al. (2022) compared multiple segmentation models, such as SegNet, UNet, PSPNet, Tiramisu, DeepLabV3+, and DeepLabV3+, with Decouple SegNet, including their proposed model, DeepLab-V3-A1. The result shows that their proposed model outperformed other methods in the Bangkok urbanscapes dataset; however, the dataset and model are not openly available.

This study uses DeepLabV3, a model from TensorFlow's DeepLab series, to segment street view images based on these model reviews. The Cityscapes dataset, which includes stereo videos recorded on the streets of more than 50 cities, pre-trains this model, making it ideal for pixel-level and instance-level semantic segmentation for urban scene detection (Cordts et al., 2016). No study has yet explored bikeability factor extraction using both SVI and non-SVI approaches, nor has any study focused on cycling route recommendations in Thailand. Bridging this gap, this study aims to: (1) create a bikeability map by extracting bikeability indicators from both SVI and non-SVI datasets; and (2) recommend the safest cycling routes for daily transportation in Kholung Toei district, Bangkok, Thailand.

Table 2.1 Literature reviews focusing on research bikeability indicators.

Title	Author	Study Area	Safety	Accessibility	Cycling Suitability	Visual Perception
Using Open Source Data to Measure Street Walkability and Bikeability in China: A case of Four Cities	Gu et al. (2018)	Tianjin, Chongqing, Kunning, Shijiazhuang (China)	- Bike lane existence - Crossing facility existence - %Bike lane with illegal parking	- Facility accessibility	- Bike lane isolation - Street network density - Crossing facility density	- %Street with tree shade
Assessing bikeability with street view imagery and computer vision	Ito and Biljecki (2021)	Singapore and Tokyo	- Number of vehicles - Presence of on-street parking - Presence of traffic lights/ stop signs - Number of speed control services	- Number of intersection with lights - Number of intersection without lights - Number of cul-de-sac - Number of POI - Number of transit facilities	- Slope - Type of road - Presence of potholes - Presence of streetlights - Presence of bike lane - Type of pavement - Presence of street amenities - Presence of utility pole - Presence of bike parking - Presence of sidewalk - Presence of crosswalk - Presence of curb cuts - Road width	- Shanon land use mix index - Air quality index - Scenery: greenery - Scenery: buildings - Scenery: water Attractiveness for cycling - Cleanliness - Beauty
A personalized bikeability-based cycling route recommendation method with machine learning	Meng and Zheng (2023)	Nanshan District, Shenzhen, Cjina	N/A	- Scenic spots - Cultural - Commercial	- Slope - Sinuosity - Cycleway - Nightlight	- Greenery - Outdoor enclosure - Crowdedness
Data-Driven Approach for Urban Micromobility Enhancement through Safety Mapping and Intelligent Route Planning	Tamagusko et al. (2023)	Lisbon, Portugal	- Bike lane - Other vehicles - Pothole - Streetlight - Trafffic light - Truck	N/A	- Parking - Pedestrian area	N/A
Using Deep Learning and Google Street View Imagery to Assess and Improve Cyclist Safety in London	Rita et al. (2023)	London	- Cycle lane - Vehicle speed - Lane width - Street lighting - Pavement quality - Tram/ train rails and water drainers - Number of intersections and intersection visibility - Lorries and other large vehicles - Advanced stop line - Bend visibility - Pedestrians	N/A	N/A	N/A

Table 2.2 Literature reviews focusing on research goals.

Title	Author	Study Area	Goal	Bikeability indicator extraction method (Non-SVI approach)	Bikeability indicator extraction method (SVI approach)	Bikeability scoring method	Route recommendation method	Research output
Using Open Source Data to Measure Street Walkability and Bikeability in China: A case of Four Cities	Gu et al. (2018)	Tianjin, Chongqing, Kunning, Shijiazhuang (China)	In this paper, the authors propose a street-score framework that can quantify not only street accessibility but also design factors for safety and comfort	N/A	- BikeScore	- Shanon's Information Entropy Weighting	N/A	- Street score map (walkability and bikeability)
Assessing bikeability with street view imagery and computer vision	Ito and Biljecki (2021)	Singapore and Tokyo	The research uses computer vision techniques extracting bikeability indicators from Google Street View	- Digital Elevation Model (DEM) - OpenStreetMap (OSM) - Land Use (LU) - Air Quality Index (AQI)	- Object detection (YOLOv3) - Image segmentation (DeepLabv3)	- Equal weighted linear combination models	N/A	- Indicator distribution map
A personalized bikeability-based cycling route recommendation method with machine learning	Meng and Zheng (2023)	Nanshan District, Shenzhen, Cjina	This research aims to propose the personalized bikeability-based cycling route recommendation method (PBCRR)	- Digital Elevation Model (DEM) - OpenStreetMap (OSM) - Point of Interest (POI)	- Image segmentation (DeepLabv3+)	- Arbitrary weighted linear combination models	- Impedance calculation	- Bikeability mp - Cycling suitability map - Visual perception map - Accessibility map - Personalized bike route recommendation
Data-Driven Approach for Urban Micromobility Enhancement through Safety Mapping and Intelligent Route Planning	Tamagusko et al. (2023)	Lisbon, Portugal	This study aims to construct a safety map and a risk-aware routing system for micromobility users in diverse urban environments	N/A	- Object detection (NVIDIA) - Image segmentation (YOLOv5)	- The "bikeable" neural network uses to assign safety score for each image	- OpenRouteService API	- Safety map - Intelligent route planner
Using Deep Learning and Google Street View Imagery to Assess and Improve Cyclist Safety in London	Rita et al. (2023)	London	The research addresses the identification of cyclists' risk factors using deep learning techniques applied to a Google Street View (GSV) imagery dataset	N/A	- Object detection (YOLOv5) - Image segmentation (PSPNet101)	- Indicators' distribution and correlation between indicators	N/A	- Indicator distribution map

2.2 Theoretical Framework

2.2.1 Graph Theory

The study of transportation and routing networks is a key application of graph theory (Martin, 2014). In graph theory, a graph consists of vertices (or nodes) connected by edges. These edges can be directed, such as one-way streets, or undirected, such as two-way streets. A common definition of a graph involves a set V of vertices. For any two elements u and v in V, the unordered pair $\{u,v\}$ represents their relationship. In this context, u and v do not need to be distinct, and the order of the elements in the pair does not matter ($\{u,v\}$, $\{u,v\}$). Unordered pairs $\{u,v\}$, where $u,v \in V$ are defined by the sett $\mathrm{Sym}(V \times V)$.

- An undirected graph (or network), $G = (V, E)$, consists of a set of vertices (or nodes) V along with an edge set $E \subseteq \mathrm{Sym}(V \times V)$ The elements of E are known as edges or links. The number of elements in V is referred to as the order of G, and we often say that G is a graph on V

Figure 2.1 An example of an undirected graph representation of E = {{1,1}, {1, 2}, {2,3}}.

- Let $G = (V, E)$ be a graph. An edge of the form $\{v, v\} \in E$ is called a loop. If G has no loops, it is referred to as a simple graph (see Figure 2.2).

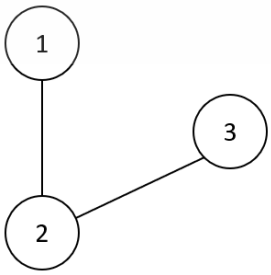

Figure 2.2 A simple undirected graph representation of E = {{1, 2}, {2,3}}.

- A directed graph, $G = (V, E)$, consists of a set V of vertices and a set $E \subset V \times V$ of edges. G is referred to as a simple directed graph if it contains no loops, whereas E elements are called directed edges. If $e = \{u, v\} \in E$ is a directed edge, then e is an edge from a starting vertex u to an ending vertex v. Figure 2.3, for directed graphs, edges are thought of as having direction, so the edge {2, 3} is considered different than the edge {3, 2}.

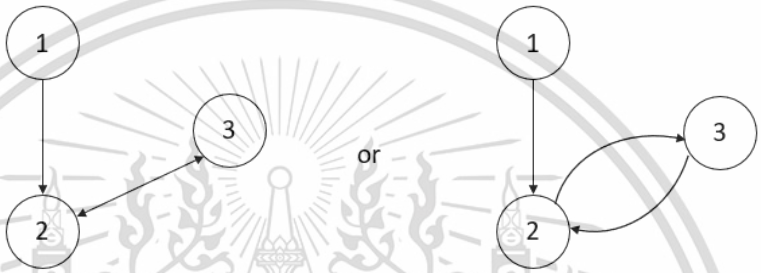

Figure 2.3 A simple directed graph representation of E = {{1, 2}, {2,3}, {3,2}}.

- A weighted graph is a (directed or undirected) graph $G = (V, E)$ with a weight function w: $E \longrightarrow R$ that assigns a weight to each edge (see Figure 2.4). A common type of weight is distance, and a path can be routed through an ordered sequence of directed edges that connects to an ordered sequence of nodes.

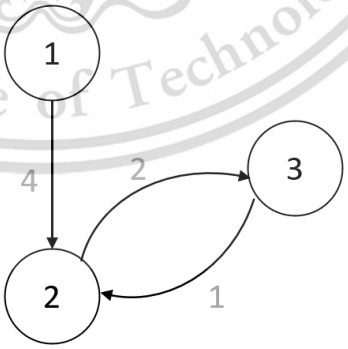

Figure 2.4 A weighted directed graph.

- Multigraphs are graphs that have multiple edges between the same vertices. If these multiple edges are directed, the graph is called a directed multigraph.

2.2.2 Representation of Street Network

As shown in Figure 2.5, there are two ways to represent networks: node-to-node, also known as a primal graph, or edge-to-edge, also known as a dual graph.

- A primal graph represents places or junctions as nodes, and roads as edges.
- A dual graph represents roads as graph nodes and the crossing points between them as edges.

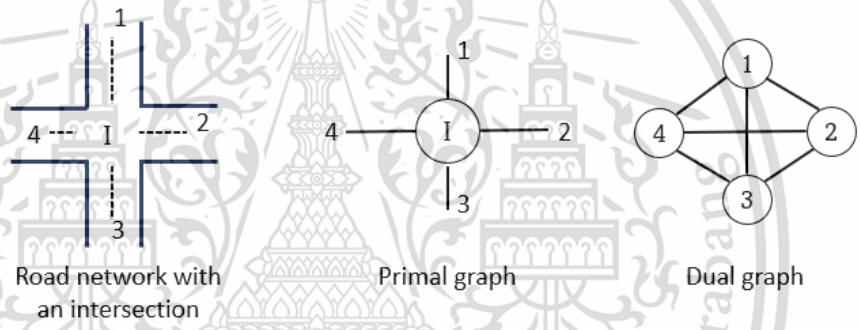

Figure 2.5 Comparison between primal and dual graphs.

Since distance is one of the most important bikeability indicators, we represent street networks as a primal graph (Lau, B.S.K. 2020).

2.2.3 OpenStreetMap

OpenStreetMap is a crowd-sourced map database that is completely free of charge and continuously updated by users. It has four main components:

- Node: A unique pair of latitude and longitude values used to map points of interest (POI) such as shops, parks, and transport stops.
- Way: A collection of two or more nodes used to map linear features like streets, rail lines, and highways.

- Relation: A representation of the relationship between components (such as nodes and ways).
- Tags: Metadata in key-value pairs, where users can freely add any information.

Chapter 3
Research Methodology

3.1 Indicator Selection and Dataset

Bikeability, which is derived from pedestrian walkability, assesses the convenience and safety of cycling environments. Researchers have developed various metrics to assess factors such as cycling infrastructure, route safety, comfort, and aesthetic appeal. These assessments utilize both street view image (SVI) methods and non-SVI methods to analyze built environment characteristics (Mamidala et al., 2019; Ito and Biljecki, 2021; Tamagusko et al., 2023; Meng and Zheng., 2023). The goal of this research is to enhance cycling safety for everyday transportation, while also considering various other factors beyond safety to increase the likelihood of selecting the recommended route (Berghofer and Vollrath, 2023; Uijtdewilligen et al., 2023).

Bangkok residents are hesitant to cycle due to several reasons: limited directness, lack of coherence, low safety, minimal comfort, and lack of attractiveness (Bakker et al., 2018). Factors like low directness and lack of coherence are unchangeable due to existing government-provided cycling infrastructure. Consequently, the bikeability score in this study is a composite of three indicators: visual perception, cycling suitability, and accessibility. Cycling suitability aims to mitigate safety risks and discomfort. Visual perception and accessibility indicators are enhancing the attractiveness of suggested cycling routes. Table 3.1 summarizes three primary indicators with corresponding sub-indicators (Dai et al., 2023; Meng and Zheng, 2023).

Table 3.1 Indicators, and corresponding sub-indicators for bikeability analysis.

	Indicator	Sub-indicator	Dataset
Bikeability	Visual perception	Greenery	SVIs
		Crowdedness	
		Outdoor enclosure	
	Cycling suitability	Sinuosity	Bike Network dataset
		Cycleway	Bikeway routes dataset from the government
		Nightlight	SVIs
	Accessibility	Attraction spots	POIs
		Commercial spots	
		Leisure spots	

3.1.1 Visual perception

This entails using street view images (SVI). Greenery is defined as the presence of street vegetation and other greenery. Crowdness measures the density of street obstructions, such as parked vehicles or street furniture. Finally, outdoor enclosures assess cyclists' perceptions of openness and spatial comfort when traveling through urban environments.

3.1.2 Cycling suitability

This assesses road sections' safety and physical comfort, taking into account factors such as sinuosity, the presence of cycle paths, and nighttime illumination. We gather data for this indicator from a bike network dataset, which contains bicycle routes in the Bangkok Metropolitan Area, and SVIs.

3.1.3 Accessibility

This looks at how many service facilities are available at destinations by using sub-indicators like leisure spots, commercial spots, and attraction spots from point-of-interest (POI) datasets.

3.2 General Framework

Figure 3.1 illustrates the proposed framework. Four stages are included. The initial stages of the framework, data acquisition, and preprocessing serve as fundamental pillars in the process of recommending safe bike routes. Subsequent stages involve the execution and analysis of research objectives, with a focus on generating bikeability maps and recommending the safest cycling routes for everyday transportation. We utilize a variety of data collection methods to ensure comprehensive insights. This includes extracting bike network data from OpenStreetMap (OSM) and sampling reference data points, with a focus on comprehensive spatial coverage. We retrieve Street View Images (SVI) data from various angles using the Google Street View Static API. Furthermore, we gather point-of-interest (POI) data to assess accessibility and categorize them into different types of spots to evaluate their distributions. We also source cycleway routes, crucial for cyclist safety, from government databases.

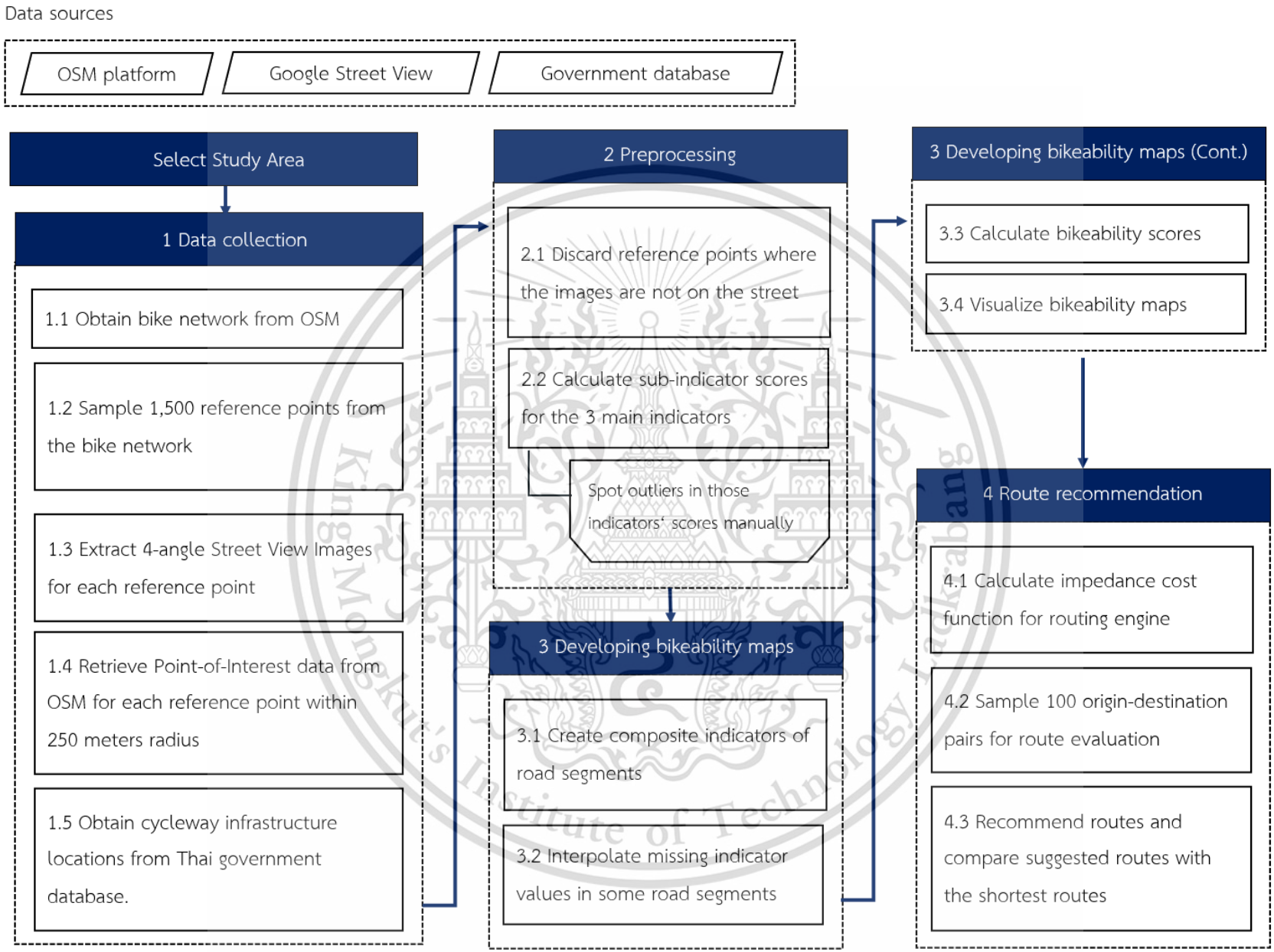

Figure 3.1 Proposed Framework

Section 3.3 will discuss the first step, data collection. Section 3.4 outlines the second step, preprocessing. Sections 3.5 and 3.6, respectively, will discuss the research's objectives—developing bikeability maps and recommending the safest routes for daily use—conducted via the third and fourth steps.

3.3 Data Collection

This section presents methodical approaches to collecting essential datasets for evaluating biking suitability. The process begins by extracting the bike network from OpenStreetMap (OSM), detailed in sub-section 3.3.1, followed by line simplification to facilitate analysis. Sub-section 3.3.2 then samples reference data points from the simplified bike network. Sub-section 3.3.3 then uses the reference points to retrieve street view images (SVI) data for street view perception. Sub-section 3.3.4 also gathers point-of-interest (POI) data. Finally, sub-section 3.3.5 discusses the Thai government database as the source of cycleway infrastructure data.

3.3.1 Obtaining Bike Network from OSM

Within the OSM platform, multiple network types are available, including walk, drive, bike, or all modes, allowing users to specify the type of street network they wish to retrieve. The pipeline utilized the Python-written OSMnx library, choosing "bike" to retrieve the bike network. This process filters out footways, steps, motorways, and private ways out of the provided network.

OSM furnishes a bicycle network structured as a bidirectional weighted graph denoted as $G = (V, E)$. $V = \{v_i\}$ constitutes the set of all vertices within graph G While $E = \{e_{i,j}\}$, where $e_{i,j} = \{v_i, v_j\}$ with $v_i, v_j \in V$, $i \neq j$, comprises the set of directed edges constituting the network's framework.

Each vertex signifies a point (or node) on the map belonging to the urban bike network. Each edge represents a road segment that connects map points (nodes) and receives a weight value based on a user-defined criterion. Thus, by definition, nodes correspond to junctions, whereas edges represent the streets connecting these junctions, as illustrated in Figure 3.2. However, the accuracy of the network often falls short of the

definition (Schmitz et al., 2008; Krenz, 2017). We then need to apply line simplification (Figure 3.3).

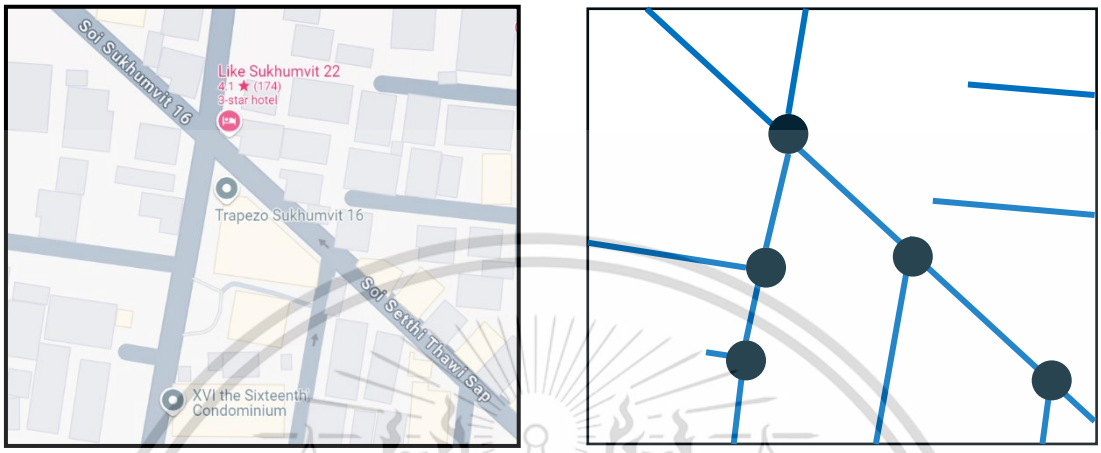

Figure 3.2 Graph representation of the bike network.

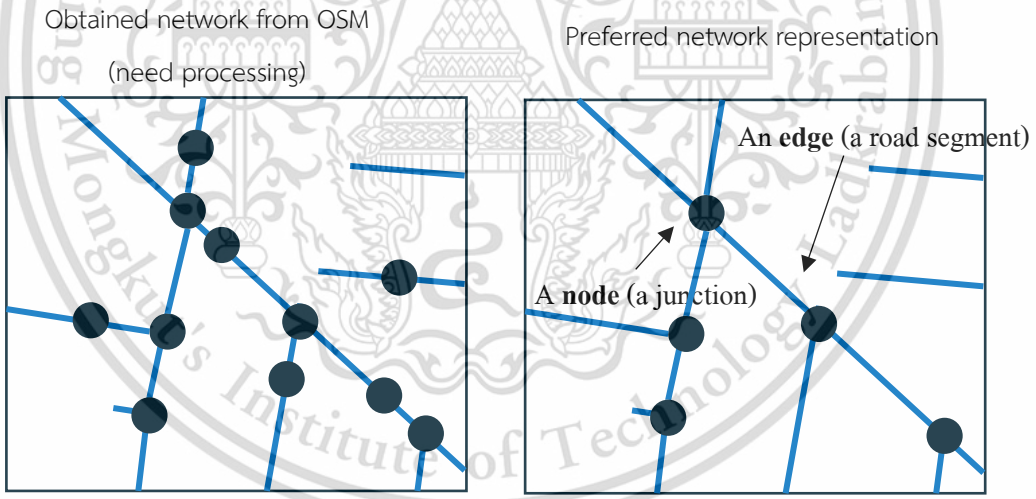

Figure 3.3 Comparing bike networks before and after line simplification processing.

3.3.2 Sampling Nodes on Each Road Segment

We will use the sampling nodes to retrieve Google Street View and POI datasets. However, due to the study's use of open-sourced datasets that guarantee free access to Google Street View Static API requests, we extracted a total of 1,500 reference data points from the simplified bike network. The process to ensure comprehensive coverage is

outlined in Figure 3.2. First, we use road names as identifiers to pinpoint midpoint locations along each road, designating them as reference points. Secondly, we randomly sample any remaining points to ensure thorough representation. We subsequently retrieve POI and SVI datasets based on these reference points. Figure 3.4 demonstrates this process by sampling 10 reference data points. We present an example bike network with 5 nodes (junctions) and 14 edges (road segments). Figure 3.4a shows that a road name can be missing, colored in blue lines, or composed of multiple road segments. Figure 3.4b prioritizes selecting five reference points by utilizing street names as keys to identify midpoint locations along the roads. Finally, we depict the random selection of the remaining 5 points.

Table 3.2 Pseudocode represents the reference data points sampling approach.

```
function sample_reference_points(simplified_bike_network):
    reference_points = []
    total_points = 1500
    for a road in simplified_bike_network:
        midpoint = find_midpoint(road)  // Find midpoint along the road
        reference_points.append(midpoint)
        total_points -= 1
    while total_points > 0:
        random_point = randomly_select_point()  // Randomly select additional
        points
        reference_points.append(random_point)
        total_points -= 1
return reference_points
```

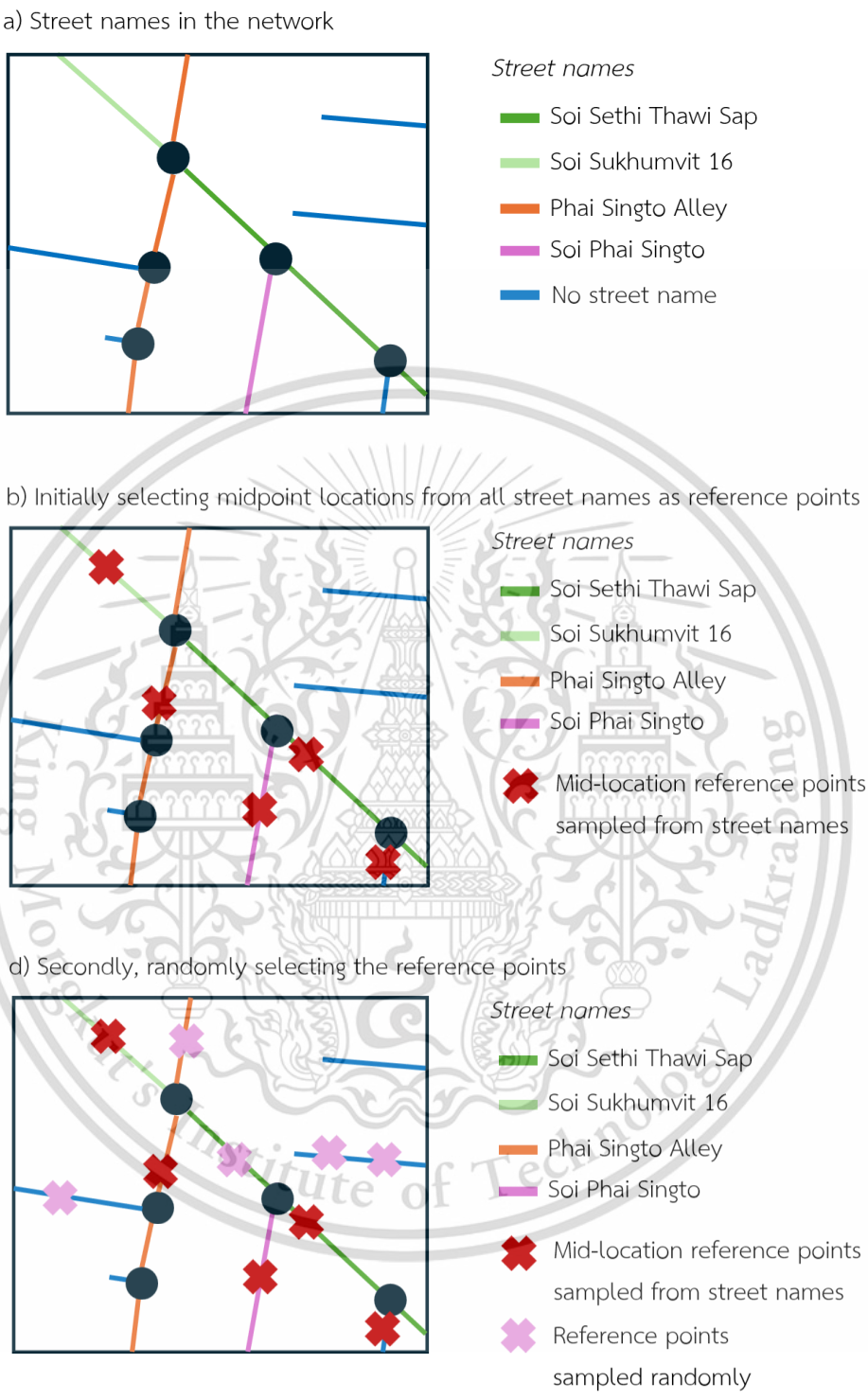

Figure 3.4 Sampling 10 reference points.

3.3.3 Extracting SVI Data for Each Reference Point

In urban studies, street-level images have proven invaluable, often used alongside semantic segmentation techniques to extract information from the images. The Google Street View Static API (exemplified in Figure 3.5) retrieves a total of four images for each reference point, each taken from a different heading: 90 degrees (true east), 180 degrees, 270 degrees, and 360 degrees, with the Field of View (FOV) set to 90, the pitch to 10, and the size to 640x640 pixels.

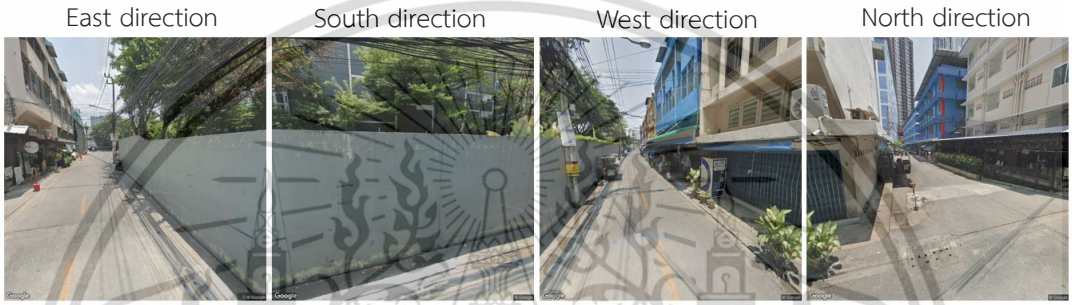

Figure 3.5 Example of 4-heading images retrieved for a complete panorama view.

Note:

1) The heading denotes the compass direction in which the camera is pointing. Accepted values range from 0 to 360 degrees, with both 0 and 360 indicating north, 90 indicating east, 180 indicating south, and 270 indicating west.
2) The FOV determines the image's horizontal field of view, acting as a zoom control. Figure 3.6 shows the degree relationship between the street view zoom level and FOV.

Street View zoom level	Field of View (degrees)
0	180
1 (default)	90
2	45
3	22.5
4	11.25

Figure 3.6 A relationship between Street view zoom level and FOV in degrees (image from Google Maps Platform).

3) Size is a numeric vector of length 2, specifying the image's output size in pixels, presented as width x height.

4) Pitch defines the angle at which the Street View vehicle positions the camera. While it is often flat and horizontal, positive values angle the camera upwards (with 90 degrees indicating straight up), while negative values angle the camera downwards (with -90 degrees indicating straight down).

3.3.4 Retrieving Point-of-Interest Data

We acquire the number of POIs within a 250-m radius of the reference point and divide them into three groups (Lee et al., 2021; Meng and Zheng, 2023): attraction spots, commercial spots, and leisure spots (see Figure 3.7) to assess accessibility.

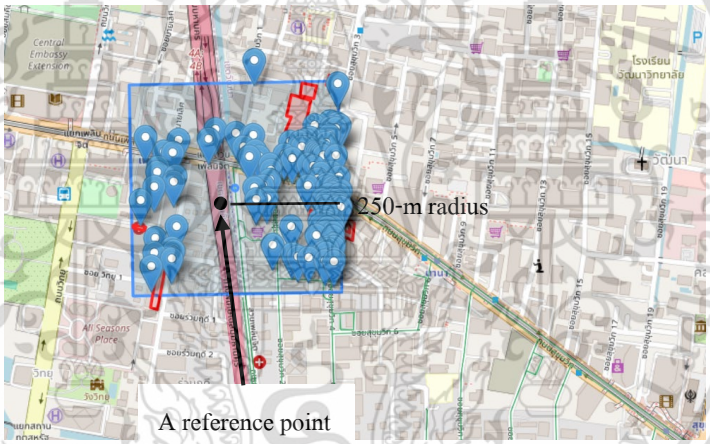

Figure 3.7 An example of POIs within a 250-m radius of a reference point.

3.3.5 Obtaining Cycleway Infrastructure

The dataset is available in shapefile format on the data.bangkok.go.th website. However, since the study area of interest may not encompass the entire region where these bikeways are located, it becomes necessary to filter the data to include only the bikeways within the study area.

3.4 Preprocessing

Data preprocessing is critical in assessing urban bikeability, serving as a foundation for data preparation and accuracy in subsequent analyses. This process involves discarding points where images do not align with roads using segmented results from a pre-trained model (detailed in sub-section 3.4.1). Afterwards, we compute sub-indicator scores for three primary indicators: visual perception, cycling suitability, and accessibility. In sub-section 3.4.2, we will discuss all the equations used for score calculation, including outlier identification, statistical analysis, and visualization.

3.4.1 Discarding Points Where Images are Not on Roads

To ensure the accuracy of our analysis, we discard points where images do not correspond to roads. Although roads change less frequently than weather patterns, occasional transformations such as maintenance activities or new road constructions do occur. Since the OSM platform functions as a crowdsourcing platform, its topographical network may not update as swiftly as larger mapping enterprise platforms like Google Maps. Hakley and Weber (2008) have also identified inaccurate road tags. Consequently, there may be instances where sampled reference points are mislocated and not situated on the intended road. Additionally, an image from Google Street View might not accurately represent a street view. Manually addressing this issue is impractical, as 4-angle images are retrieved from 1,500 reference points, resulting in a total of 6,000 images to review.

To address this, we employ a pre-trained semantic segmentation model that detects whether images, based on their reference points, are located on roads. Given that the obtained images may depict indoor or outdoor locations, we select a comprehensive model. We use an open-source encoder-decoder model trained on the ADE20K scene parsing dataset, which includes 150 semantic categories, encompassing both indoor and outdoor images, as illustrated in Figure 3.8. By identifying the absence of road classes in the segmented images, we can accurately determine which points should be discarded, ensuring they are correctly located on roads.

Figure 3.8 Examples of both indoor and outdoor images from the ADE20K dataset.

3.4.2 Calculating Sub-Indicator Scores

Table 3.3 summarizes the extraction methods for the sub-indicators that make up the three main indicators.

Table 3.3 Methods used to extract sub-indicator components for score calculation.

	Indicator	Sub-indicator	Dataset	Extraction method
Bikeability	Visual perception	Greenery	SVIs	Semantic segmentation
		Crowdedness		
		Outdoor enclosure		
	Cycling suitability	Sinuosity	Bike Network dataset	Sinuosity calculation
		Cycleway	Bikeway routes dataset	Bikeway mapping
		Nightlight	SVIs	Semantic segmentation
	Accessibility	Attraction spots	POIs	Buffer analysis
		Commercial spots		
		Leisure spots		

3.4.2.1 Visual perception

The visual perceptibility indicator heavily relies on SVI segmentation, utilizing the open-source DeeplabV3 model pre-trained on the Cityscapes dataset. This dataset

includes stereo videos recorded on the streets of over 50 different cities, making the model well-suited for pixel-level and instance-level semantic segmentation in urban scene detection (Cordts et al., 2016). The model classifies 19 different labels.

To assess cyclists' perception, we consider three sub-indicators. Greenery measures the proportion of street vegetation in the image, Crowdedness represents the amount of street obstructions, and Outdoor Enclosure reflects the ratio of vertical elements, such as buildings, walls, and trees, to horizontal features like sidewalks and roads. In this study, these sub-indicators are calculated by counting pixel values corresponding to 14 specific classes, as shown in equations (1), (2), and (3).

$$\text{Greenery}^{p} = \frac{\sum_{h=1}^{n} T_h^p}{n \times \text{Total number of pixels}} \quad (1)$$

$$\text{Crowdedness}^{p} = \frac{\sum_{h=1}^{n} O_h^p}{n \times \text{Total number of pixels}} \quad (2)$$

$$\text{Outdoor enclosure}^{p} = \frac{\sum_{h=1}^{n} B_h^p + \sum_{h=1}^{n} T_h^p}{\sum_{h=1}^{n} S_h^p + \sum_{h=1}^{n} R_h^p + \sum_{h=1}^{n} F_h^p} \quad (3)$$

Where:

h is an individual split of street view images (h = 1, 2, 3, 4 which corresponds to a heading of 90°, 180°, 270° and 360°)

n is the number of headings acquired (4 in this research)

T_h^p is an integer number of trees in pixels (segmented class: vegetation and terrain) of an image with heading, **h**, at a reference point, **p**.

O_h^p is an integer number of obstacles in pixels (segmented class: person, rider, car, truck, bus, train, bicycle, and motorcycle) of an image with heading, **h**, at a reference point, **p**.

B_h^p is an integer number of segmented class buildings in pixels of an image with heading, **h**, at a reference point, **p**.

S_h^p is an integer number of segmented class sidewalks in pixels of an image with heading, **h**, at a reference point, **p**.

R_h^p is an integer number of segmented class roads in pixels of an image with heading, **h**, at a reference point, **p**.

F_h^p is an integer number of segmented class fences in pixels of an image with heading, **h**, at a reference point, **p**.

3.4.2.2 Accessibility

The density of points of interest (POI), defined by Lee, J. et al. (2021) as the number of POIs within a 250-m radius of the reference point, determines sub-indicators of accessibility. In OSMWe acquire around 100 categories of POI in OSM tags, but in this study, we classify POI tags into three sub-indicators: attraction, commercial, and leisure, as listed in Table 3.4. tion is defined as the number of green spaces and tourist attraction spots. Commercial includes restaurants and various types of shops. Relaxation spots and educational establishments define leisure. The detailed calculation for each category is as in equations (4), (5), and (6).

$$\text{Attraction}^{p} = \sum \text{POI Attraction}^{p}_{\text{category}} \quad (4)$$

$$\text{Commercial}^{p} = \sum \text{POI Commercial}^{p}_{\text{category}} \quad (5)$$

$$\text{Leisure}^{p} = \sum \text{POI Leisure}^{p}_{\text{category}} \quad (6)$$

Where:

$\text{POI Attraction}^{p}_{\text{category}}$ is an integer number of places with a POI category, **i**, in a 250-m radius of a reference point, **p**, corresponding to the attraction sub-indicator, see Table 3.4.2.2.

Attraction^{p} is a summation of places with all categories in a 250-m radius of a reference point, **p**, corresponding to the attraction sub-indicator.

$\text{POI Commercial}^{p}_{\text{category}}$ is an integer number of places with a POI category in a 250-m radius of a reference point corresponding to the commercial sub-indicator.

Commercial^{p}	is a summation of places with all categories in a 250-m radius of a reference point corresponding to the commercial sub-indicator.
$\text{POI Leisure}^{p}_{\text{category}}$	is an integer number of places with a POI category in a 250-m radius of a reference point corresponding to the leisure sub-indicator.
Leisure^{p}	is a summation of places with all categories in a 250-m radius of a reference point corresponding to the leisure sub-indicator.

Table 3.4 POI categories retrieval from the OSM platform relevant to each sub-indicator.

Sub-indicators	POI categories
Attraction	planetarium', 'park', 'department_store', 'mall', 'travel_agency
Commercial	platform', 'station', 'stop_position', 'atm','bank','bar', 'bicycle_parking','bicycle_rental', 'bus_station', 'cafe', 'childcare', 'cinema', 'clinic', 'community_centre', 'dentist', 'doctors', 'fast_food', 'food_court', 'hospital', 'ice_cream', 'marketplace', 'nightclub', 'pharmacy', 'place_of_worship', 'pub', 'restaurant', 'spa', 'theatre', 'veterinary', 'art', 'bag', 'bakery', 'beauty', 'beverages', 'bicycle', 'books', 'cannabis', 'car', 'car_parts', 'car_repair','chemist', 'clothes', 'coffee', 'computer', 'confectionery', 'convenience', 'copyshop', 'cosmetics', 'doityourself','electronics', 'erotic', 'furniture', 'general', 'gift', 'greengrocer', 'hairdresser', 'hardware', 'health_food', 'hifi', 'interior_decoration', 'jewelry', 'laundry', 'massage', 'motorcycle', 'musical_instrument', 'optician', 'photo', 'scuba_diving', 'second_hand', 'sewing', 'shoes','sports', 'supermarket', 'tailor', 'tattoo', 'tea', 'toys', 'trade', 'tyres', 'variety_store', 'video_games'
Leisure	amusement_arcade', 'dog_park', 'fitness_centre', 'garden', 'golf_course', 'pitch', 'playground', 'sauna', 'sports_centre', 'stadium', 'swimming_pool', 'kindergarten', 'language_school', 'school', 'university'

3.4.2.3 Cycling suitability

Three distinct sub-indicators divide the assessment of cycling suitability: sinuosity, presence of cycleways, and nightlight availability. Sinuosity quantifies the curvature of the road, computed as the ratio between the straight line, the Euclidian distance of the road segment, and the actual road length. If the Bangkok bikeway dataset lists a road segment's location as having a cycleway, it is considered to have one. Furthermore, the nightlight sub-indicator assigns the presence of streetlights to a road segment. The pole class infers these streetlights from the segmented street view images, which correspond to their respective road segments. Equations (7), (8), and (9) represent the calculation methods.

$$\text{Sinuosity}^{r} = \frac{\text{Road Length}^{r}}{\sqrt{(x_2^r - x_1^r)^2 - (y_2^r - y_1^r)^2}} \quad (7)$$

$$\text{Cycleway}^{r} = \begin{cases} 0 & \text{, if bikeway does not exist} \\ 1 & \text{, if bikeway exists} \end{cases} \quad (8)$$

$$\text{Nightlight}^{p} = \begin{cases} 0 & \text{, if class pole is not found in the segmented image} \\ 1 & \text{, if class pole is found in the segmented image} \end{cases} \quad (9)$$

Where:

Road Length^{r}	is the actual distance of a road segment **r**.
$(x_1^r, y_1^r), (x_2^r, y_2^r)$	are latitudes and longitudes at both ends of a road segment.
Sinuosity^{r}	is a degree of road curvature.
Cycleway^{r}	is a representation of the bikeway existence of a reference point **p**.
Nightlight^{p}	is a representation of the nightlight existence of a reference point **p**.

3.4.2.4 Outlier identification

In the process of outlier identification, the calculated sub-indicator scores undergo thorough analysis and visualization techniques to find potential anomalies. This crucial step involves utilizing descriptive statistics and examining the data distributions. By

employing statistical measures such as mean, median, standard deviation, and range, researchers can gain insights into the central tendency and variability of the scores. Additionally, researchers utilize graphical representations like histograms, box plots, and bar plots to visualize the data distribution and identify any unusual patterns or deviations from the norm. By accurately identifying outliers, researchers can ensure the integrity and reliability of the analysis, leading to more accurate conclusions and insights drawn from the data.

3.5 Developing Bikeability Maps

The scope of developing bikeability maps, which is one of the research purposes, requires a structured approach. The first is to normalize and average sub-indicator scores assigned to reference points or road segments into indicator scores (sub-section 3.5.1). We then interpolate missing indicator scores using inverse-distance weighted (IDW) interpolation, ensuring that all road segments have values for the bikeability calculation (sub-section 3.5.2). Next, we calculate the bikeability score of the roads using a weighted combination of accessibility, visual perception, and cycling suitability indicators (sub-section 3.5.3). Finally, we visualize urban visual perception, cycling suitability, accessibility, and bikeability on the maps, offering spatial insights into the study area (sub-section 3.5.4).

3.5.1 Compositing Indicators Calculation of Road Segments

We average the scores of pertinent sub-indicators from all reference points on the same road segment to determine an indicator's score for that road segment. However, we independently assess each sub-indicator's score. Given that these sub-indicators may have differing scales, normalization is necessary to standardize the scores before averaging. Equation (10) outlines the normalization technique, transforming the scores into a range of 0 to 1 while preserving the data distribution. This normalization also considers the impact of the sub-indicator on cyclists, where a positive sub-indicator indicates that a higher value enhances cycling activity, while a negative sub-comparator has the opposite effect. Equation (11) shows the averaging of a road segment.

$$\text{norm } SI_k^r = \begin{cases} \dfrac{SI_k^r - \min SI_k}{\max SI_k - \min SI_k}, & \text{positive sub-indicators} \\ \dfrac{\max SI_k - SI_k^r}{\max SI_k - \min SI_k}, & \text{negative sub-indicators} \end{cases} \quad (10)$$

$$I_j^r = \frac{\sum_1^n \text{norm } SI_k^r}{\text{Total number of reference points}} \quad (11)$$

Where:

SI_k^r is a value of sub-indicator **k** of a road segment **r**.

$\min SI_k$ is the minimum value of a sub-indicator **k** considering all road segments?

$\max SI_k$ is the maximum value of a sub-indicator **k** considering all road segments?

$\text{norm } SI_k^r$ is a normalized value of sub-indicator **k** of a road segment **r**.

I_j^r is a value of indicator **j** (j = attraction, accessibility, and visual perception) of a road segment **r**.

Greenery, cycleways, nightlight existence, and accessibility are all positive sub-indicators. While sinuosity and crowdedness are considered negative, Incidentally, the outdoor enclosure sub-indicator poses a challenge due to its unique nature. We consider values within 1.6 as positive, indicating that outdoor enclosures offer cyclists a comfortable experience. However, values exceeding 1.6 are considered negative (Tran et al., 2020).

3.5.2 Interpolating Missing Indicator Scores

Missing indicator values on a road segment might happen due to the process of point discarding and outlier removal. For bikeability score calculation and map visualization, each road segment must contain a value. Multiple spatial urban studies (Shiode and Shiode, 2009; Achilleo, 2011; Ismain et al., 2023) have robustly utilized the inverse-distance weighted (IDW) interpolation technique. IDW computes the value of an unknown location by assigning weights based on the distance between the unknown point and its neighboring data points, with closer points receiving higher weights. Figure 3.9

illustrates the process of interpolating an unknown indicator of a road segment using five neighbors. Equation (12) provides the IDW calculation (GISGeography, 2024).

$$\text{Interpolated indicator}_j^r = \frac{\sum_{i=1}^{n} \left(\frac{\text{indicator}_i^j}{d_i^2}\right)}{\sum_{i=1}^{n} \left(\frac{1}{d_i^2}\right)} \quad (12)$$

Where:

n	is the number of the nearest neighborhood used for interpolation (5 in this research).
indicator_i^j	is a representation of the known value of indicator **j** of a neighborhood **i.**
d_i	is the distance between a neighborhood **i** and the target point.
$\text{Interpolated indicator}_j^r$	is the interpolated value of indicator **j** which is a representation value for the road segment **r**.

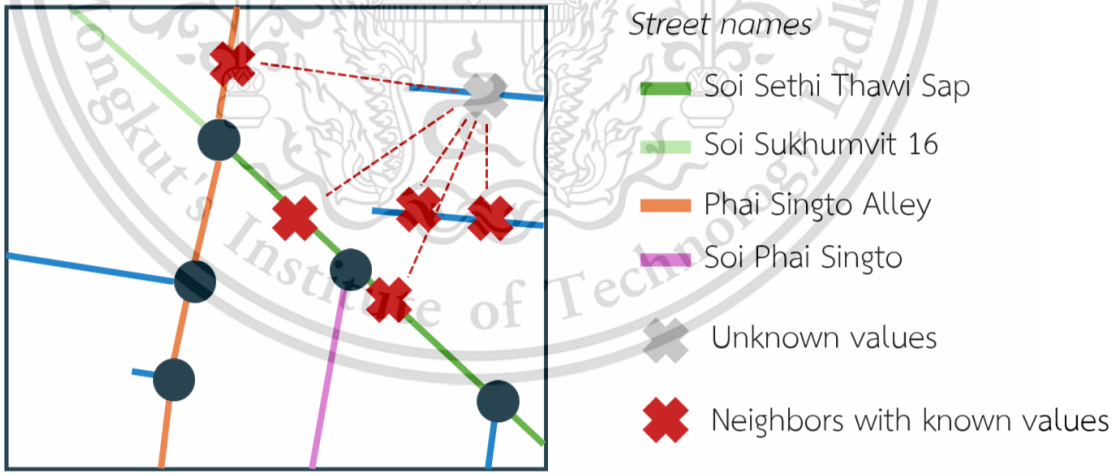

Figure 3.9 Inverse-Distance Weighted interpolation with 5 neighbors.

3.5.3 Calculating Bikeability Score Tailored to Daily Use

The route recommendation cost function (discussed in Section 3.6) is based on bikeability scores. In determining bikeability, a weighted linear combination is a common

method (Santos et al., 2022; Meng and Zheng, 2023). Therefore, we use a weighted combination of the three main indicators, as shown in Equation (13).Meng and Zheng (2023) suggest weights of 0.07, 0.31, and 0.62 for accessibility, visual perception, and cycling suitability, respectively, for bicyclists aiming for commuting (or daily) modes of transport in China. Karolemeas et al. (2022) consider different indicators for bikeability scores in Greece. However, the author's research concludes that the weights for accessibility, visual perception, and cycling suitability are 0.11 for activity coverage, 0.33 for natural-and-built environments, traffic-and-junction density, and 0.56 for the remaining indicators. A survey of cycling experts supports these weights, ranking the importance of variables in descending order. Street characteristics such as cycling infrastructure, green pathways, and other facilities are considered less important (Hardinghaus and Nieland, 2021). Thus, this study adopts the weights and method from Meng and Zheng (2023) for bikeability score calculation.

$$B_r = w_A I_A^r + w_V I_V^r + w_C I_C^r \quad (13)$$

Where: `

I_A^r, I_V^r, I_C^r are the accessibility, **A**, visual perception, **V**, and cycling suitability, **C**, indicators' value of a road segment, **r**, respectively.

w_A, w_V, w_C are the weights of accessibility, visual perception, and cycling suitability indicators.

B_r is the bikeability score of a road segment.

3.5.4 Visualizing Bikeability Maps

Maps visualize the spatial distributions of the three primary indicators: accessibility, visual perception, and cycling suitability.

3.6 Recommending Safe Bike Route for Daily Use

In urban route planning, minimizing a cost function, known as impedance, is essential for efficient route optimization. Different factors such as travel distance, speed, and time

can calculate the impedance function. This study generates a bike impedance function for bike route recommendation purposes, as explained in sub-section 3.6.1. Sub-section 3.6.2 uses randomly generated origin-destination pairs within a 3-kilometer radius to simulate real-world scenarios for route recommendation and evaluation.

3.6.1 Calculating Impedance Function

When proposing a route, a cost function must be defined to determine the route with the lowest score. Transportation agencies often utilize traffic impedance as a quantitative measure of road weights, serving as a cost function. Factors such as travel distance, speed, and time reflect the ease or difficulty of traveling along a road segment. Conventional road networks typically employ the length of road segments as a measure of traffic impedance (Li et al., *2023).* However, in the context of bicycle road networks, additional criteria come into play. While the length of road segments remains relevant, other factors are also considered. Meng and Zheng (*2023)* offer an approach to calculating the impedance score using the actual road length and the road's bikeability score, as shown in equation *(*14*)*.

$$\text{Impedance}_r = \frac{\text{Length}_r^{n_L}}{B_r^{n_B}} \quad (14)$$

Where:

Length_r	is the actual distance of a road segment **r**.
B_r	is the likeability score of a road segment.
n_L, n_B	are the nth power of Length_r and B_r , indicating whether cyclists prioritize the shortest distance or environmental factors.
Impedance_r	is the impedance value of a road segment.

In this research, 1 and 2 will be used for n_L and n_B creating a context of cyclists paying more attention to their surroundings.

3.6.2 Sampling Origin-Destination Pairs

According to Panthasen et al. (2021), given Bangkok's hot and humid weather conditions, the greatest potential for transitioning from motorized to non-motorized transport lies within a 3-kilometer radius. Therefore, this study randomly generates 100 origin-destination (OD) pairs where the Euclidean distance between each pair does not exceed 3 kilometers, as shown in Figure 3.10.

Figure 3.10 A sample from the generated Origin-Destination pairs.

3.6.3 Recommending and Evaluating Routes

Route planning studies commonly and extensively utilize the Dijkstra algorithm due to its suitability for determining the shortest path between two points and its broad applicability in the transportation field (Dong and Shen, 2013; Sembiring et al., 2018; Kurniawan et al., 2024). The shortest path refers to the path in a weighted graph that minimizes the sum of weights along the path. Interpreting the weight as the length of a street represents the shortest distance between the path's origin and destination. Alternatively, if the weight is considered a cost, it signifies the least-cost path from the origin to the destination (Dong and Shen, 2013). As a result, this study implements the

Dijkstra algorithm in the route recommendation engine, using impedance scores as weights.

We commonly assess the resulting recommended paths by comparing them with benchmark paths (Kayler and Mazimpaka, 2016; Tamagusko et al., 2023; Meng and Zheng, 2023), usually using the shortest paths. We employ two methods from Meng and Zheng (2024) for path comparison: differences (equation 15) and similarity (equation 16).

$$\text{Difference}_{OD} = \frac{\text{Length}_{OD}}{\text{ShortestLength}_{OD}} \quad (15)$$

$$\text{Similarity}_{OD} = \frac{\text{IntersectLength}_{OD}}{\text{Length}_{OD}} \quad (16)$$

Where:

Length_{OD} is the actual distance (from the recommended path) between origin O and destination D.

$\text{ShortestLength}_{OD}$ is the shortest distance (from the shortest path) between the origin and destination.

Difference_{OD} is a measure of the difference between the recommended path and the shortest-distance path of an origin-destination pair.

$\text{IntersectLength}_{OD}$ is the total length of road segments intersecting between the recommended route and the shortest route.

Similarity_{OD} is a measure of similarity between the recommended path and the shortest-distance path of an origin-destination pair.

Chapter 4

Result and Discussion

4.1 Study area

The research's case study zooms in on the Khlong Toei district, nestled within Bangkok's Sukhumvit area in Thailand. Covering a total area of 13 square kilometers, Khlong Toei has a diverse range of land uses, including residential, commercial, industrial, recreational, utility, facility, and mixed-use areas. Various modes of transportation, including bus stops, elevated train stations, and subway stations, serve the district (Iamtrakul et al., 2023). This combination of factors makes Khlong Toei an ideal setting for bikeability studies, as displayed by its boundaries in Figure 4.1.

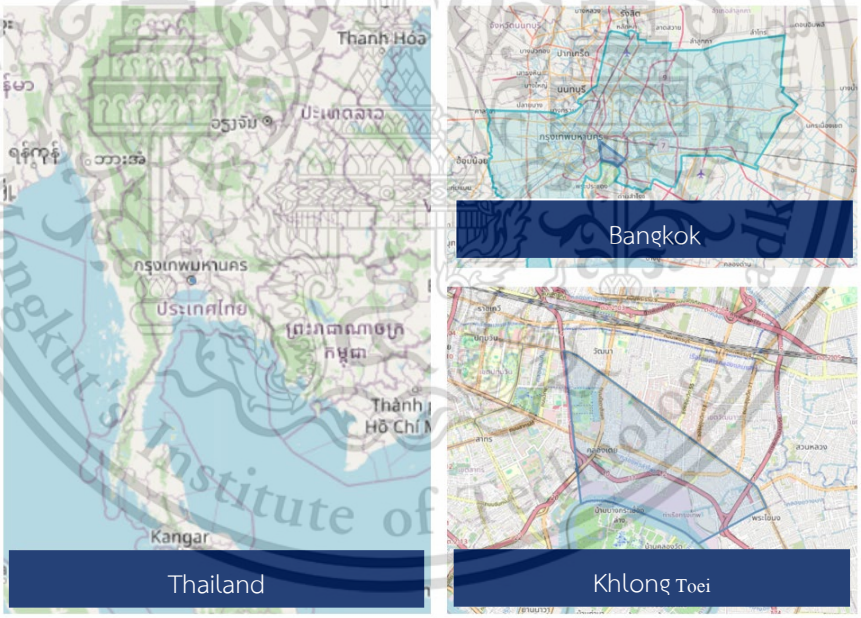

Figure 4.1 Study area, Khlong Toei district.

4.2 Results

This section contains 12 sub-sections detailing the results obtained at each stage of the study. Sub-section 4.2.1 begins with the data collection process, showcasing Khlong Toei's bike network from the OSM platform. The bike network's reference point sampling

results are in sub-section 4.2.2. For each reference point, the results of 4-angle street view images and the density of POI data are illustrated in sub-sections 4.2.3 and 4.2.4, respectively. Sub-section 4.2.5 shows the Bangkok bikeway gathered from the Thai government database.

Sub-section 4.2.6 investigates the invalid not-on-road reference points during the preprocessing stage. We then statistically and visually analyzed the calculated sub-indicator scores to identify outliers in sub-section 4.2.7.

The research conducted and obtained the objectives under sub-sections 4.2.8 to 4.2.12. Recalling the research's objectives, the first is to develop bikeability maps in Khlong Toei district, and the second is to recommend the safest cycling routes for daily commute usage. Sub-section 4.2.8 summarizes the composite indicator scores of road segments, commencing from the development stage of the bikeability map. We imputed the missing indicator scores from the previous process using IDW interpolation, resulting in sub-section 4.2.9. We then calculated and visualized the finalized bikeability scores in sub-sections 4.2.10 and 4.2.11. We investigated and evaluated the recommended routes in the last sub-section 4.2.12 by comparing them with the shortest-distance routes.

4.2.1 Obtaining Bike Network from OSM

We derived the bicycle network from the OSM dataset, filtering out road types unsuitable for bicycles. We logically excluded road types deemed unsuitable for cycling in Khlong Toei, such as motorways, motor links, and steps. Notably, some road segments with footways or residential types were also excluded. Figure 4.2a depicts the deleted footways as skywalks that prohibit bicycles. Figure 4.2b shows that the excluded residential roads are private areas.

a) Skywalks where cycling is prohibited

b) Private areas unsuitable for cycling

Figure 4.2 Examples of cycling-unsuitable roads.

The bicycle network initially contains 14,975 edges and 7,827 nodes displayed in blue lines (Figure 4.3, top). However, the retrieved edges and nodes do not denote street segments and junctions correctly. Figure 4.3 (bottom) illustrates a zooming area showing incorrect results for edges and nodes from the graph definition (edge = road segment, node = junction). Therefore, we need to simplify the lines to eliminate unnecessary street segments and non-junction nodes.

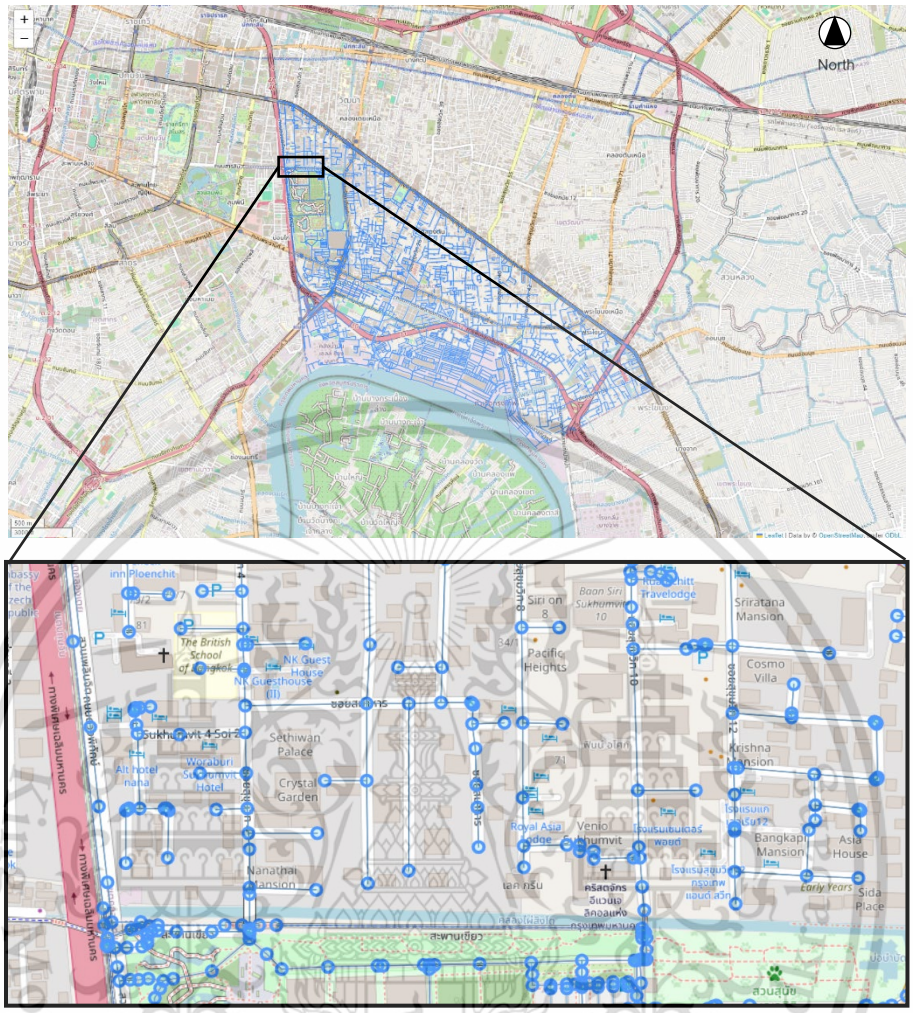

Figure 4.3 An example of incorrect edges and nodes obtained from the OSM platform.

A built-in function from the OSMnx library, a Python implementation, implemented the line simplification, resulting in a simplified bike network, as shown in Figure 4.4 (top). The simplified network comprises 4,229 edges and 1,784 nodes, indicating a reduction of more than half compared to the non-simplified version. Figure 4.4 (bottom) is a zooming area for a clear perception of the simplified edges and nodes. We primarily attribute this reduction to the removal of non-junction nodes and some road sections. The removed road segments are considered acceptable since they are unconnected to other road sections or dead ends.

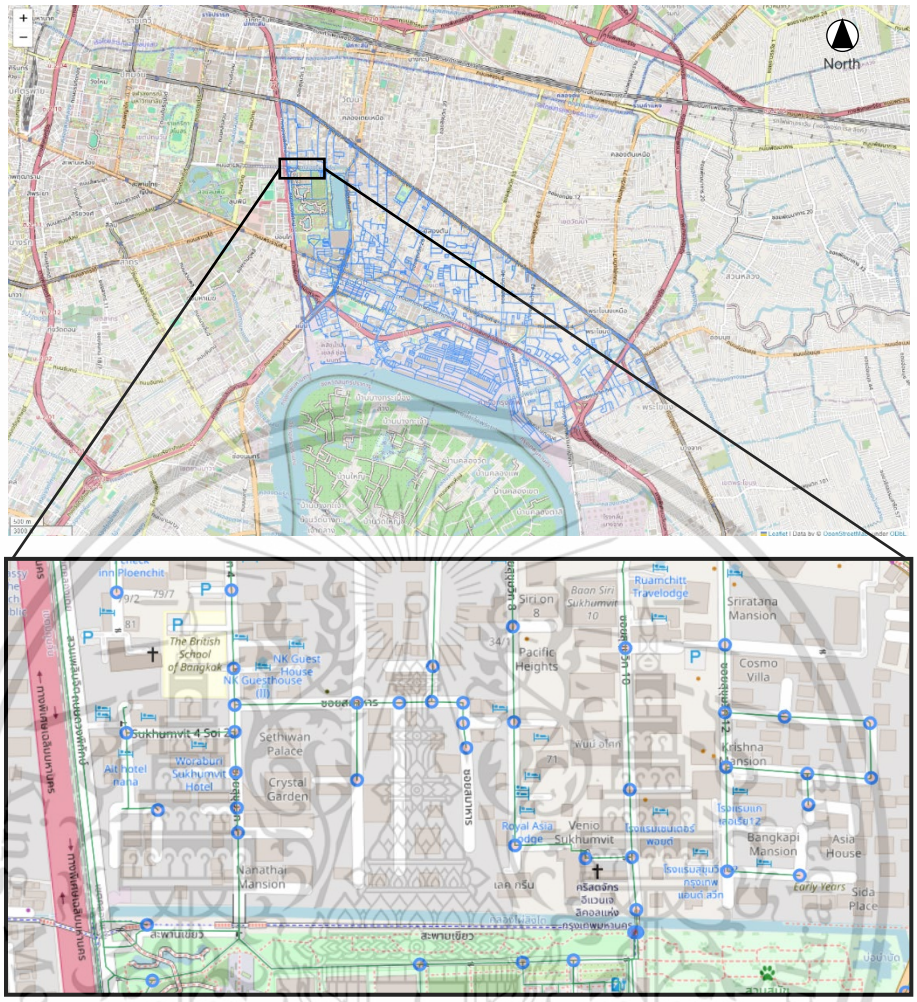

Figure 4.4 An example of (more) correct edges and nodes of the simplified network.

4.2.2 Sampling Nodes on Each Road Segment

We selected 1,500 data points from the simplified bike network for both SVI and POI data collection. Hence, thorough sampling of the bike network is essential to ensuring comprehensive research outcomes. We address the issue by implementing the following steps:

1) The midpoint locations along each road, chosen as the reference and

2) We randomly sample any remaining points to ensure a thorough representation.

In terms of spatial coverage, visualizing the sampled points in red (Figure 4.5) implies that the method effectively sampled the reference points from the bike network.

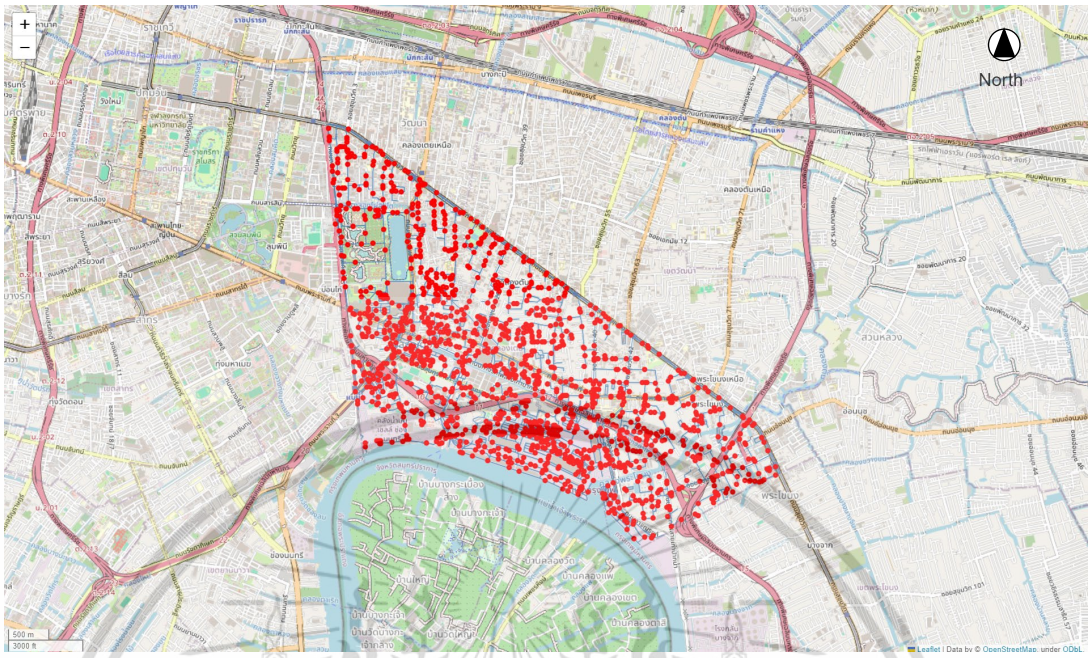

Figure 4.5 Coverage of 1500 sampled reference points.

4.2.3 Extracting SVI Data for Each Reference Point

The Google Street View Static API retrieved four street-level images with different headings: 90, 180, 270, and 360 degrees. These four images complete the total view around the reference point. However, not all 1,500 reference points are available or exist in the Google databases, as indicated by the metadata from Google API responses (Figure 4.6).


```
{
    "copyright": "© PASCAL DANNEAU",
    "date": "2019-01",
    "location": {"lat": 13.7394648, "lng": 100.5534559},
    "pano_id": "CAoSLEFGMVFpcE9rVmJYMjZKajFXREhMUTBCZHRJRk9xNXFraFdWQjBsZklWRWwt",
    "status": "OK",
}
```


Figure 4.6 An instance of Google Street View metadata response.

We return the metadata responses in JSON format, which include copyright details, the photo's capture date, location coordinates (latitude and longitude, which also serve as the API input), the pano_id key for image retrieval, and the availability status of the image. We indicate the status as "OK" when we find a panorama at the requested location.

Out of 1,500 reference points, 1,216 received an "OK" status from the Google Street View API metadata, confirming their validity. Consequently, we retrieved images from these 1,216 valid points. Furthermore, 70% of the available images were captured in 2022, whereas less than 10% were taken before 2016, as depicted in Figure 4.7. This analysis ensures a relatively up-to-date representation of the roads.

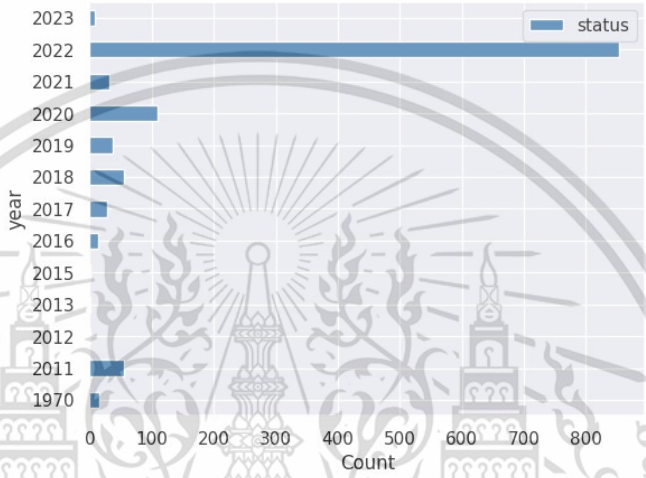

Figure 4.7 Number of images at reference points taken each year.

4.2.4 Retrieving Point-of-Interest Data

We collected the number of POI categories within a 250-m radius of the reference point and divided them into three sub-indicators. Table 4.1 shows examples of five valid reference points denoted with their corresponding POI numbers in each sub-indicator, namely: attraction, commercial, and leisure.

Table 4.1 Examples of POI density retrieved for each reference point.

longitude	latitude	Img_status	num_leisure	num_commercial	num_attraction
100.5508956	13.74218908	OK	3	152	30
100.5510134	13.74091501	OK	5	188	36
100.5513058	13.73817582	OK	5	59	33
100.5513184	13.73752924	OK	5	34	30
100.5514422	13.73633314	OK	3	12	19

4.2.5 Obtaining Cycleway Infrastructure

The Thai government database's bikeway infrastructure data is scattered and unconnected across the Bangkok area, as shown in Figure 4.8. The Traffic and Transportation Department last updated this data on February 17, 2013. This implies that there will be no further cycleway infrastructure investment after the latest investment in 2012, as stated in the NHA resolution. This dataset only retains the bikeways within the Khlong Toei district for analysis, given that the study area is part of the district.

Figure 4.8 Bikeway distribution across Bangkok, Thailand.

4.2.6 Discarding Points Where Images are Not on Roads

Given the available SVI reference points, some may not accurately represent street view characteristics. Manually verifying each of the 4,864 images (1,216 reference points multiplied by four headings) is impractical. To address this, a preliminary solution involves using a pre-trained segmentation model trained on the indoor and outdoor images. We selected this model due to the uncertain nature of the obtained images, which could potentially include indoor images. We then manually reviewed the 52 segmented images without the "Road" class. Figure 4.9 shows all 52 invalid points as black dots, with an example (latitude: 13.705201187840052, longitude: 100.60033644235588) illustrating the

segmented result. The segmented image lacks the "Road" class, indicating indoor features like ceiling, light, wall, and floor. As a result, we have reduced the number of valid on-road reference points to 1,164.

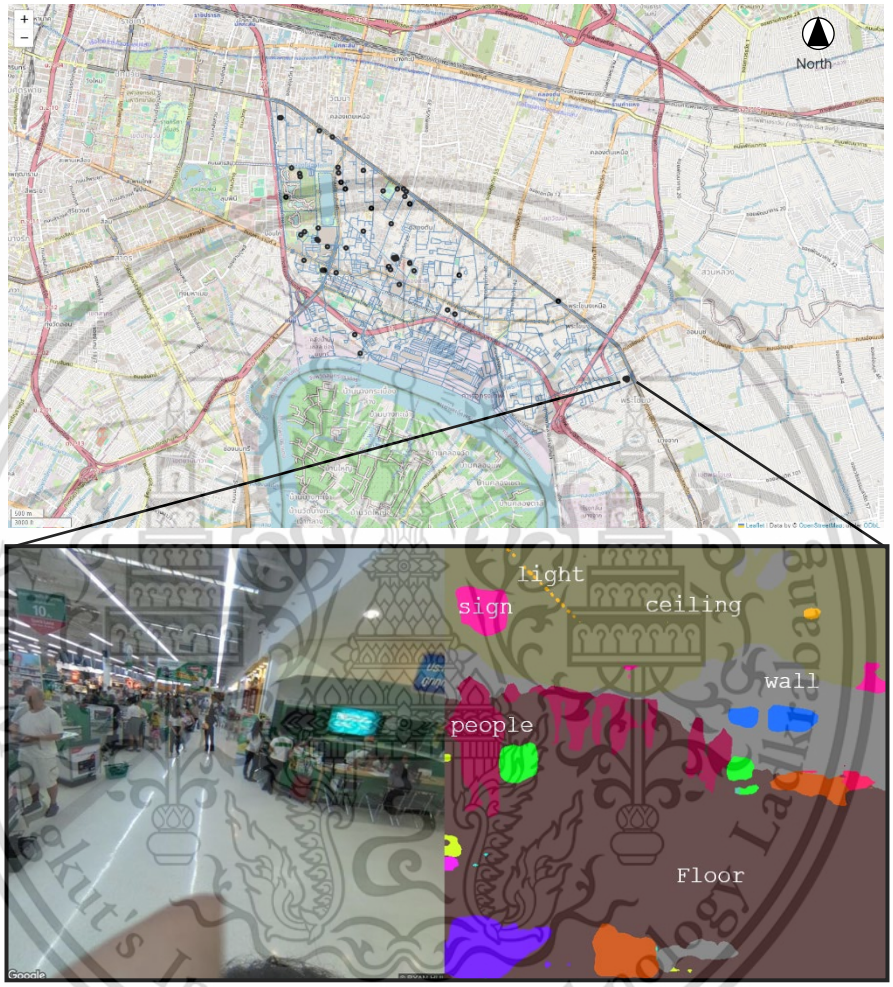

Figure 4.9 Locations where SVIs were not captured on the roads.

4.2.7 Calculating Sub-Indicator Scores

4.2.7.1 Visual perception

DeeplabV3, a different model from before, segmented four SVIs for each reference point into 19 classes using its pretraining knowledge on the Cityspaces dataset. We calculated the pixel summations for each segmented class by aggregating the pixel counts across all the images (Figure 10). The figure suggests that street view characteristics in

Khlong Toei, Bangkok, are predominantly comprised of six main components: roads, buildings, vegetation, cars, sidewalks, and fences.

Khlong Toei, one of Bangkok's central business areas, creates a landscape filled with diverse road types and various building (commercial) structures, contributing to these results. In Thailand, it is common to see vegetation alongside or in the middle of roads, often provided by the government. Additionally, due to the mixed-land use of the area, not only commercial but also residential buildings have established themselves. Residential areas typically have vegetation surrounding the houses, and people commonly use fences to enclose them for safety and privacy reasons.

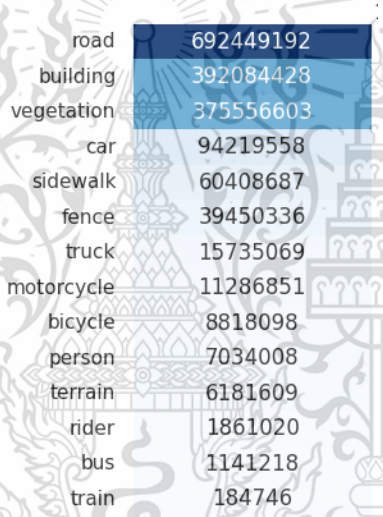

Figure 4.10 The summation of the number of pixels for each class.

Equations (1), (2), and (3) in Chapter 3 would process and average all four segmented images (varying headings: 90, 180, 270, and 360 degrees) using Figure 4.11 as an example. Although the segmented boundaries of each class may not be precisely defined, the overall segmented components are considered satisfactory. The road class (depicted in purple) is typically situated in the middle and lower halves of the images. ATypically, the middle and lower halves of the images house the road class (depicted in purple). r prominent component is the buildings (dark gray) distributed throughout the image, primarily outside the road class.

However, images captured under specific lighting conditions may cast shadows onto the road, potentially leading to misinterpretation in some instances. Additionally, when bikeable roads are located beneath a motorway, the image displays multiple results, including instances of unreasonableness in the upper half. Unreasonable instances include certain objects, such as roads, sidewalks, vehicles, or pedestrians. Figure 4.12 illustrates the misinterpretation of the car (blue) and sidewalk (pink) classes in the upper half of the street-level images, which deviates from typical street-view characteristics. Moreover, fences underneath the motorway also lead the model to mislabel unused streets underneath the motorway as sidewalks. Note that the sample location is at latitude 13.715640266617935 and longitude 100.5549227105012.

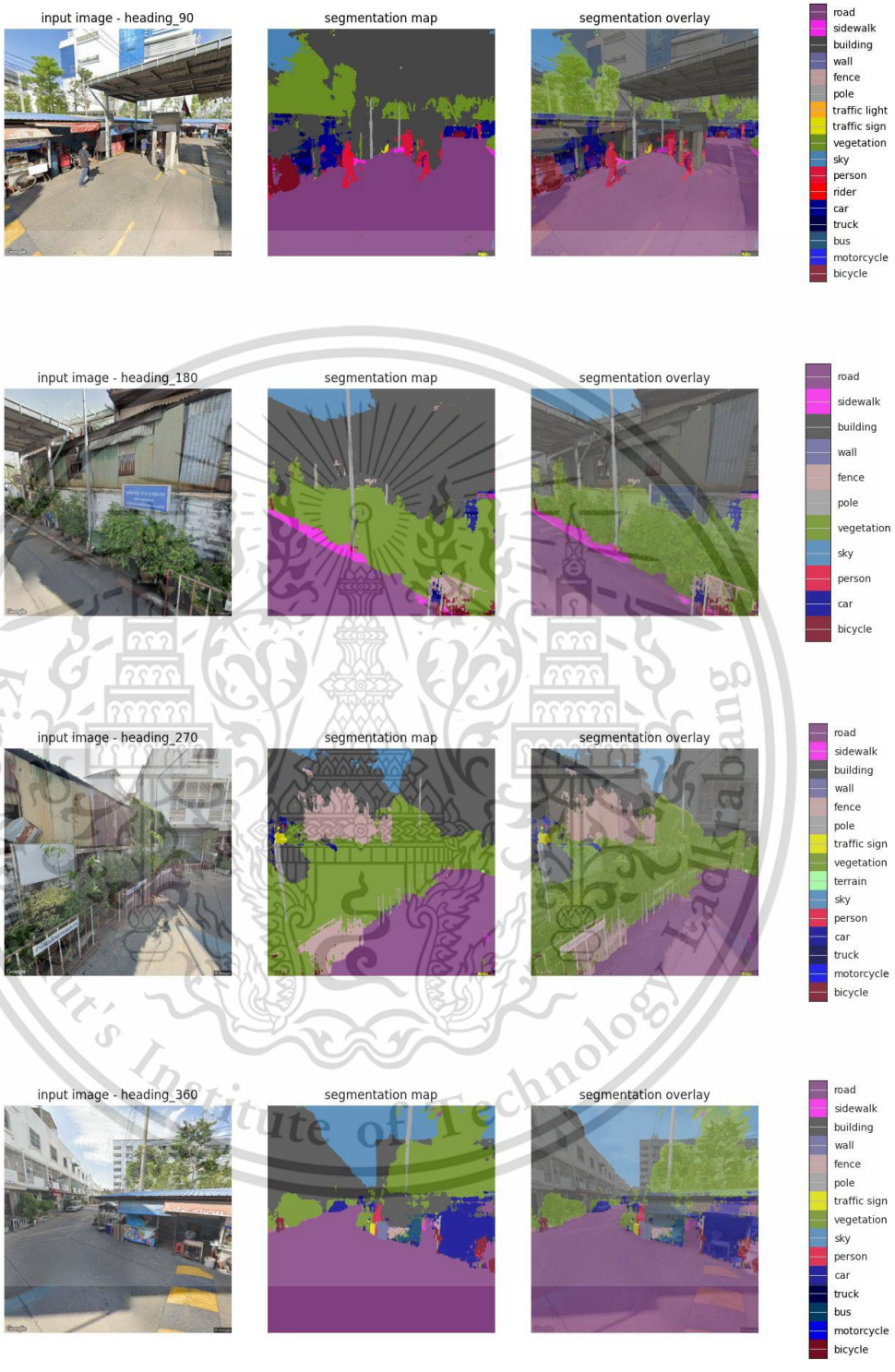

Figure 4.11. Examples of four-angle segmented street view images.

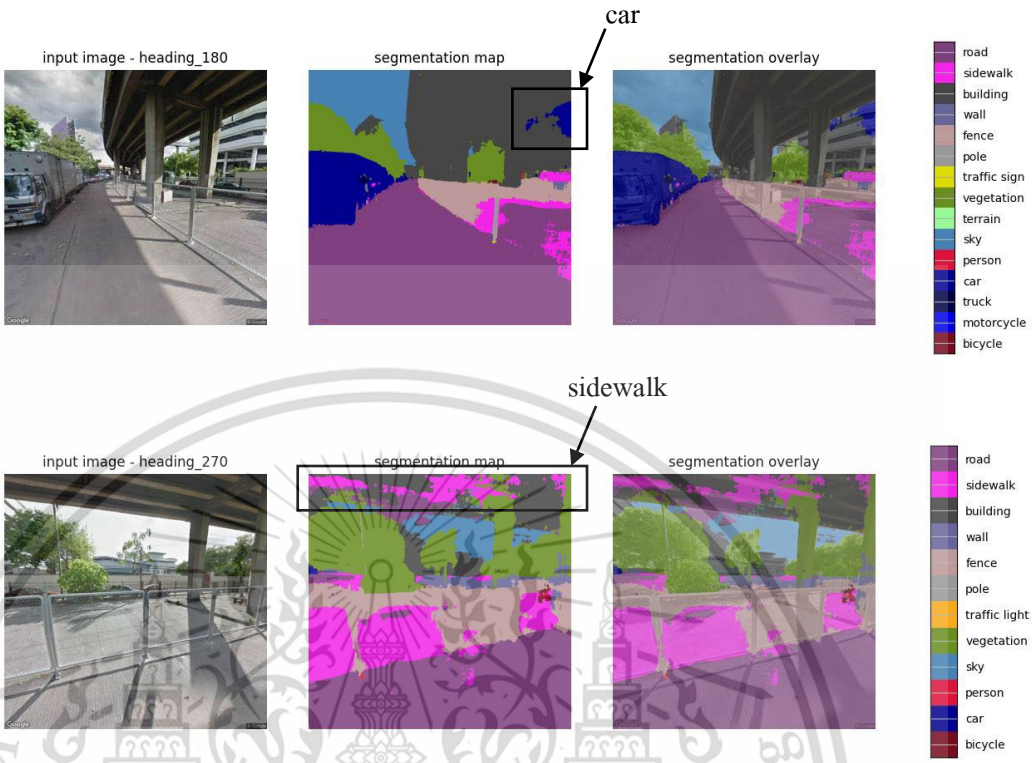

Figure 4.12 Examples of unreasonable objects in the upper half of the images.

We calculated the segmented classes based on greenery, crowdedness, and outdoor enclosures. Figure 4.13 visualizes the score distribution of these categories using boxplots. Notably, Outdoor Enclosure exhibits a significantly higher value (around 100) compared to the majority of values within its category. Further investigation revealed that the obtained images at five locations fail to accurately depict the street view. Figure 4.14 depicts the capture of some images from tall buildings during the night. As a result, we removed these five reference points, bringing the total number of reference points down to 1,159.

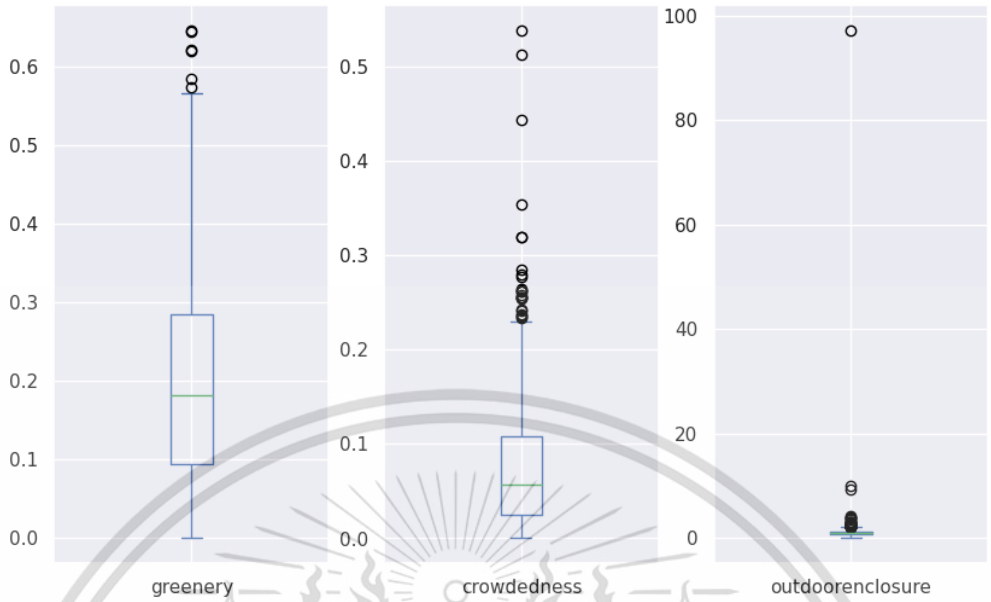

Figure 4.13 Score distribution of visual perception category with outliners in the outdoor enclosure.

Latitude: 13.729681603058337 Longitude: 100.55592537598996

Figure 4.14 Examples of non-road-representing street view images.

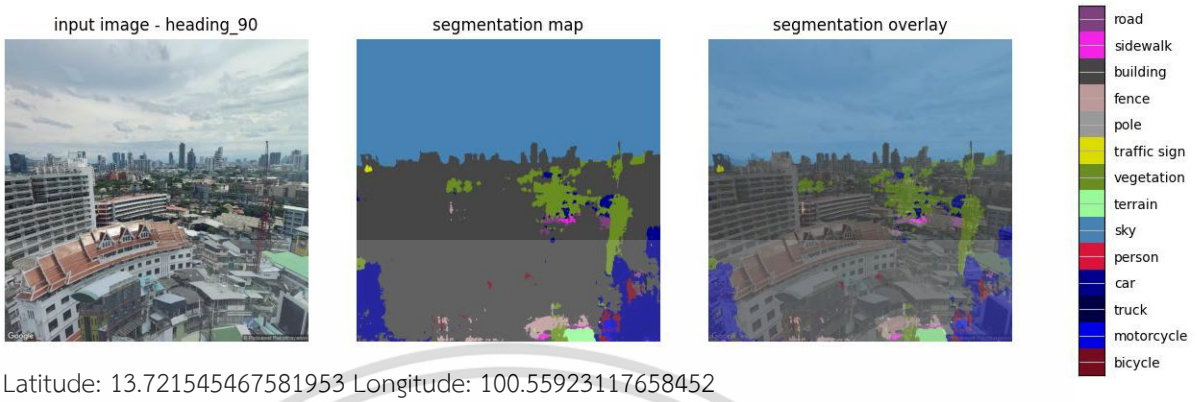

Latitude: 13.721545467581953 Longitude: 100.55923117658452

Latitude: 13.710721893396004 Longitude: 100.5653152

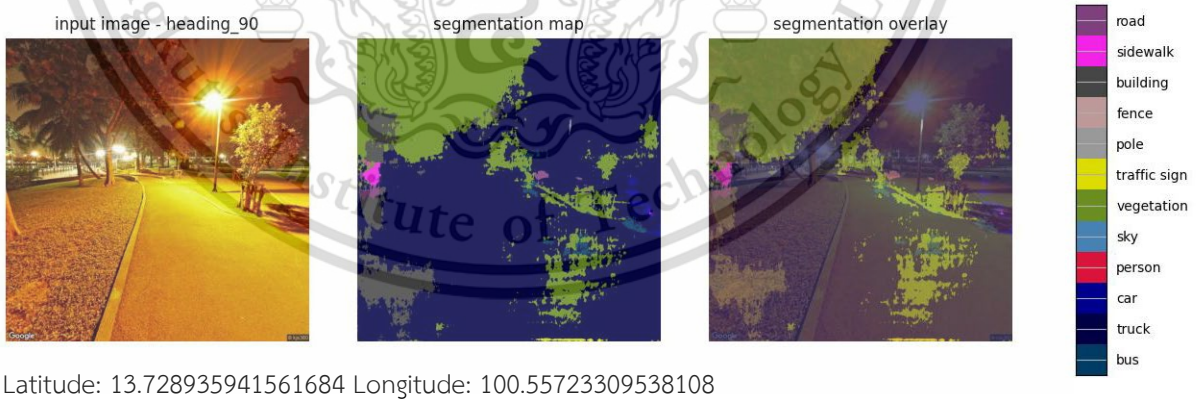

Latitude: 13.728935941561684 Longitude: 100.55723309538108

Figure 4.14 Examples of non-road-representing street view images (Cont.).

4.2.7.2 Accessibility

Buffer analysis assesses the sub-indicators of accessibility. This involves assigning the number of points of interest (POI) within a 250-meter radius of each reference point, categorized into attraction spots, commercial spots, and leisure spots (Table 4.2).

Table 4.2 Descriptive analytics of POI density (Total number of reference points = 1,159).

	num_attraction_poi	num_commercial_poi	num_leisure_poi
count	915.0	1090.0	917.0
mean	7.05	25.51	3.5
std	9.96	39.69	2.82
min	0.0	1.0	1.0
25%	1.0	5.0	1.0
50%	3.0	11.0	2.0
75%	7.0	25.0	5.0
max	59.0	246.0	16.0

As observed in the table above, the count values for all POI densities in each category do not reach 1,159. Since some reference locations do not have any places or tags falling into those categories, This suggests that there are no attractions, commercial establishments, or leisure points at these particular reference points, resulting in an imputed value of zero. Consequently, the Khlong Toei district, being a business center, is dense with commercialized places (mean value of 25.51), while leisure spots, such as educational areas or public-sharing spots, are the least dense.

4.2.7.3 Cycling suitability

Sinuosity is the first sub-indicator examined in the cycling suitability indicator. We calculate this metric by dividing the actual length of the road segment by the straight-line distance between its endpoints. Sinuosity values range from 1 to infinity, with 1 representing a perfectly straight road segment and infinity indicating a highly curved or enclosed structure of the road segment (refer to Figure 4.15).

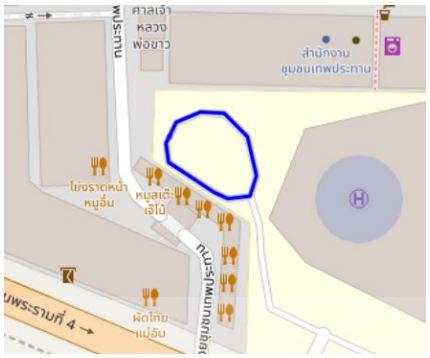

Figure 4.15 An example of an enclosed road segment.

Infinite values are not suitable for further analysis. We replace infinity values with 39.501009, the maximum observed value of sinuosity across the study area, to address this issue. Table 4.3 provides descriptive statistics of road segments' curvatures. Since 75% of the road segments have sinuosity values less than 1.07, we quote most of them straight.

Table 4.3. Descriptive analytics of sinuosity (Total number of road segments = 4,220).

	sinuosity
count	4220.0
mean	1.173395
std	1.555023
min	1.000000
25%	1.000000
50%	1.000097
75%	1.067519
max	39.501009

The second sub-indicator, cycleway, signifies whether road segments intersect with bikeways listed in the government database, with a value of 1 denoting intersection and 0 indicating absence in the bikeway database. In the analyzed area, only 162 road sections

out of 4,220, represented by green lines in Figure 4.16, have cycleways. The figure demonstrates the presence of cycleways in Benchakitti Park, where they connect to the Sukhumvit main road in a northerly direction, but they remain disconnected in other areas. Every reference point detects pole classes in terms of nightlight, suggesting illumination of all road segments during the dark hours.

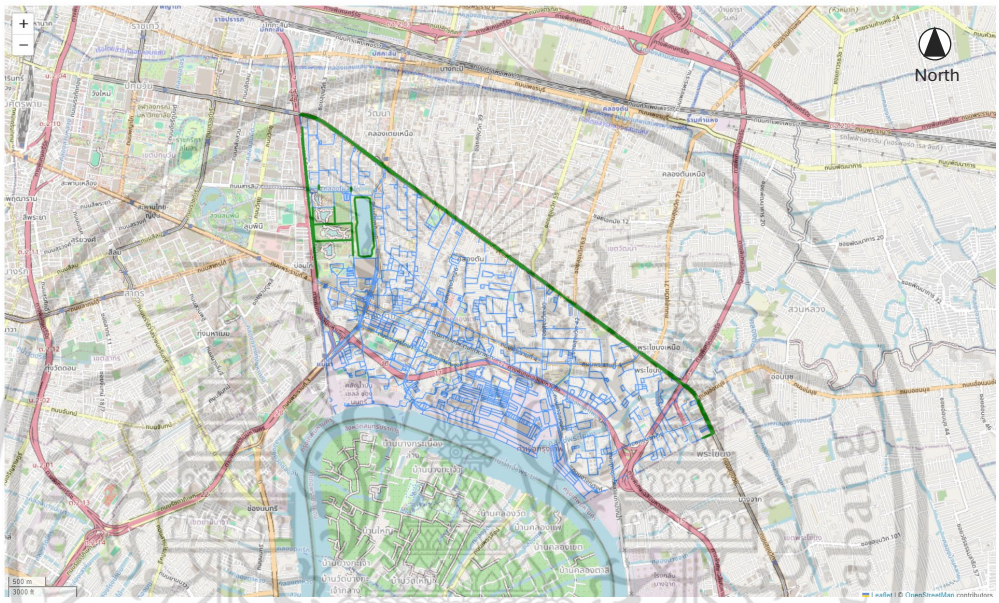

Figure 4.16 Road segments with cycleway represented in green.

4.2.8 Compositing Indicators Calculation of Road Segments

The bikeability score of a road segment in this study is the weighted average encompassing three primary indicators: visual perception, accessibility, and cycling suitability. Each road segment receives these indicators based on the average scores of their respective sub-indicators. Given the potential variance in scale among sub-indicator scores, normalization is crucial to standardize the scores before averaging. Chapter 3's equation (10) demonstrates the normalization method. Table 4.4 presents descriptive statistics for the normalized sub-indicator scores, ensuring that all scores are within the range of 0 to 1. Notably, for negative sub-indicators like crowdedness and sinuosity, the minimum normalized score corresponds to the maximum crowdedness or sinuosity score. Conversely, for positive sub-indicators like greenery, the maximum normalized score

represents greenery's highest score. Table 4.5 shows the descriptive statistics for the averaged indicators assigned to each road segment using equation (11).

Table 4.4 Descriptive statistics of normalized sub-indicators (Number of road segments = 4,220).

Indicator	Sub-indicators	count	mean	std	min	25%	50%	75%	max
Visual perception	greenery_norm	1012.0	0.31	0.2	0.0	0.15	0.28	0.44	1.0
	crowdedness_norm	1012.0	0.86	0.12	0.0	0.8	0.9	0.95	1.0
	outdoorenclosure_norm	1012.0	0.25	0.13	0.0	0.17	0.22	0.3	0.62
Accessibility	num_attraction_poi_norm	1012.0	0.09	0.16	0.0	0.02	0.03	0.1	1.0
	num_commercial_poi_norm	1012.0	0.1	0.16	0.0	0.02	0.04	0.09	1.0
	num_leisure_poi_norm	1012.0	0.19	0.2	0.0	0.07	0.14	0.28	1.0
Cycling suitability	sinuosity_norm	4220.0	1.0	0.04	0.0	0.998	0.999	1.0	1.0
	nightlight_norm	4220.0	0.24	0.43	0.0	0.0	0.0	0.0	1.0
	cycleway_norm	4220.0	0.04	0.19	0.0	0.0	0.0	0.0	1.0

Table 4.5 Descriptive statistics of averaged indicators (Number of road segments = 4,220).

Indicator	count	mean	std	min	25%	50%	75%	max
visual_perception	1012.0	0.47	0.1	0.14	0.4	0.46	0.54	0.82
accessibility	1012.0	0.13	0.14	0.0	0.03	0.08	0.17	0.72
cycling_suitability	4220.0	0.42	0.16	0.0	0.33	0.33	0.66	1.0

The highlighted cells in Table 4.5 indicate that there are 1,012 road segments with visual perception and accessibility scores (which should be equal to the entire road segment,

4,220). The deletion process, during which reference points failed to obtain suitable street view images, resulted in this reduction in the number of segments. Consequently, the next step involves applying a solution to impute the missing values.

4.2.9 Interpolating Missing Indicator Scores

The Inverse-Distance Weighted (IDW) interpolation technique interpolates the missing indicator values on a road, allowing the distances of neighboring points to the unknown location to directly influence the interpolated value. This step ensures that all road segments have complete sets of indicator scores, as shown in Table 4.6. With the inclusion of interpolated values, the descriptive statistics undergo slight changes. This implies that interpolation using this technique rarely affects the initial score distributions.

Table 4.6 Descriptive statistics of the interpolated indicators (Number of road segments = 4,220).

Indicator	count	mean	std	min	25%	50%	75%	max
visual_perception	4220.0	0.47	0.08	0.14	0.41	0.46	0.52	0.82
accessibility	4220.0	0.11	0.13	0.0	0.03	0.06	0.14	0.72
cycling_suitability	4220.0	0.42	0.16	0.0	0.33	0.33	0.66	1.0

4.2.10 Calculating Bikeability Score

The bikeability score serves as the foundation for the route optimization cost function. We derive this score through a weighted combination of three indicators: visual perception, accessibility, and cycling suitability. Based on the assumption that routes are recommended for daily use, the weights assigned to these indicators are 0.31, 0.07, and 0.62, respectively. Figure 4.17 displays the score distributions. Visual perception exhibits a relatively normal distribution, with the majority of normalized values falling between 0.41 (quantile 1) and 0.52 (quantile 3). In contrast, accessibility displays a right-skewed

distribution, suggesting that there are areas with dense point-of-interest (POI) concentrations, while other areas have fewer POIs. Additionally, cycling infrastructure has a significant impact on cycling suitability scores, resulting in a bimodal distribution. Cycleways cluster scores around 0.7, while other scores cluster around 0.3. Consequently, the weighted bikeability score tends to have a bimodal distribution aligned with cycling suitability, given its high contributing weights. On the other hand, accessibility scores do not significantly affect bikeability scores because of their low contribution to daily use purposes.

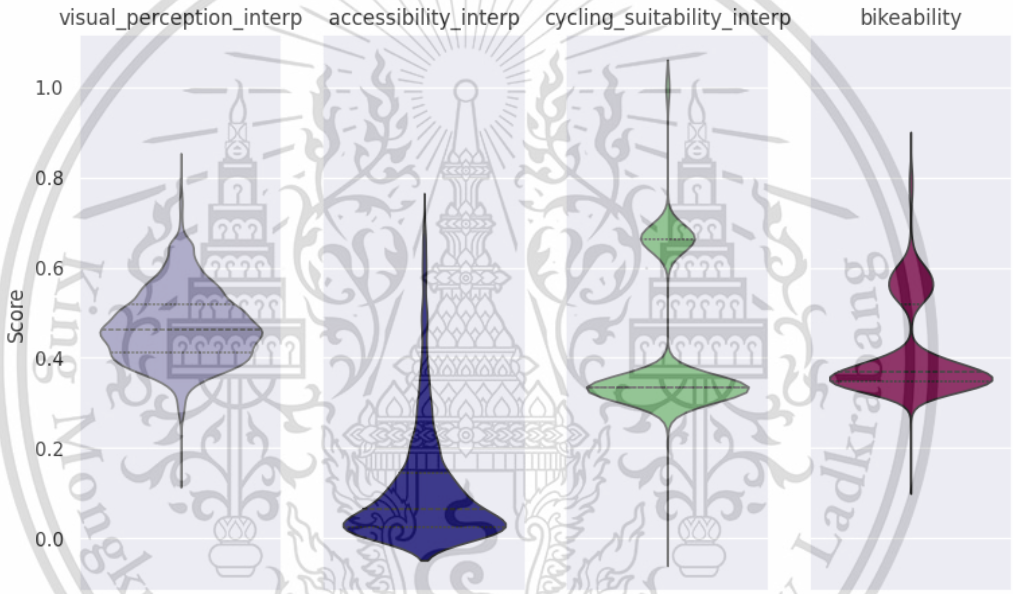

Figure 4.17 Violin plots for the three indicators and the bikeabillity scores.

4.2.11 Visualizing Bikeability Maps

Figures 4.18, 4.19, and 4.20 depict map representations of the three indicators, while Figure 4.21 presents the bikeability map. Visual perception, as illustrated in Figure 4.18, reveals lower values along main roads like Sukhumvit Road, situated at the northernmost part of the street network, and Duang Phithak Road, situated at the westernmost part of the network. Local and non-main streets exhibit high perception values. The northwestern region of Khlong Toei, which connects with other central business districts, concentrates point-of-interest dense areas, as Figure 4.19 illustrates. However, accessibility appears to be lower in residentially dense areas. These insights suggest that areas near main roads

exhibit high accessibility scores, leading to high levels of crowdedness and a low visual perception score.

In terms of cycling suitability, as observed in Figure 4.20, areas with cycleways exhibit significantly higher scores compared to other areas. Additionally, the low curvature of some streets, likely due to the presence of nightlights on every street, contributes significantly to their high cycling suitability scores. Figure 4.21 finally displays the bikeability map for daily use objectives, which is crucial in determining routes for bicyclists. Notably, streets with good bikeability scores, illustrated in dark green with scores higher than 0.7, are typically those with cycleways. In contrast, streets in lighter green generally have high visual perception scores, such as those found in Benjakitti Park. On the other hand, streets shown in dark pink are enclosed-structure streets, indicating paths that are extremely unsuitable for utility cyclists. The majority of streets fall into the 0.3–0.4 score range. This suggests that bimodal cycling suitability scores have a significant influence on bikeability score calculations. Cycleways influence the highest scores, while sinuosity and enclosure affect the lowest ones. Since these two are sub-indicators of the cycling suitability indicator, Cycling suitability obscures visual perception and accessibility issues, making them less noticeable on the visualized map.

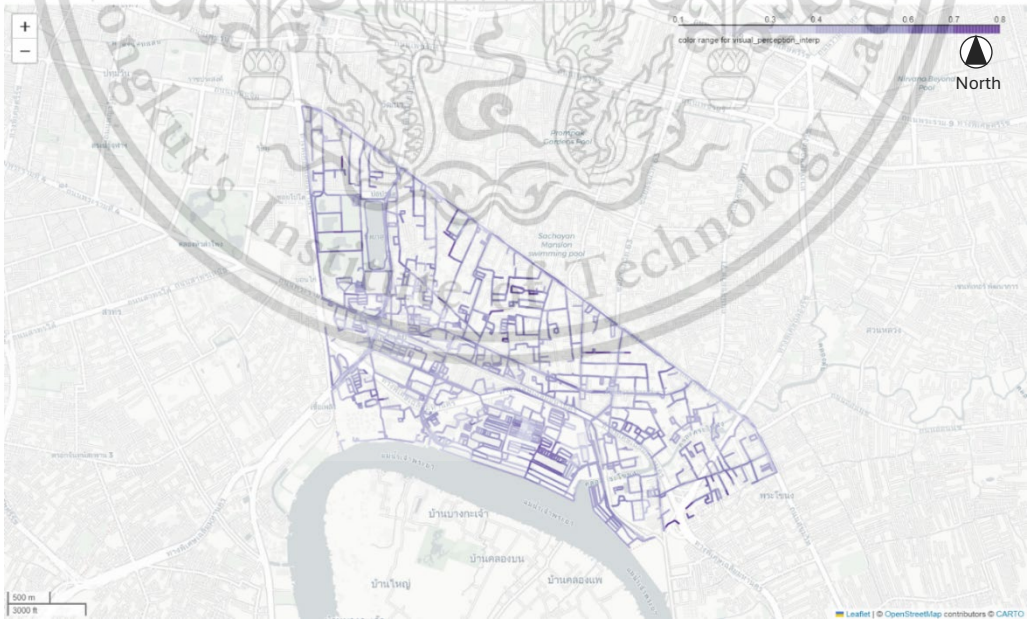

Figure 4.18 Visual perception score map.

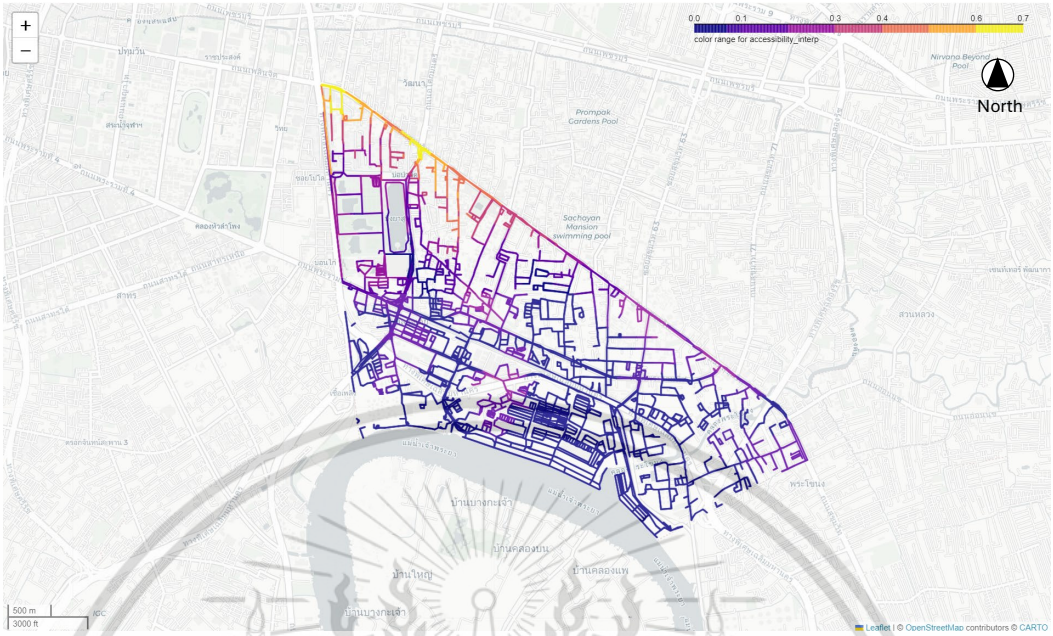

Figure 4.19 Accessibility score map.

Figure 4.20 Cycling suitability score map.

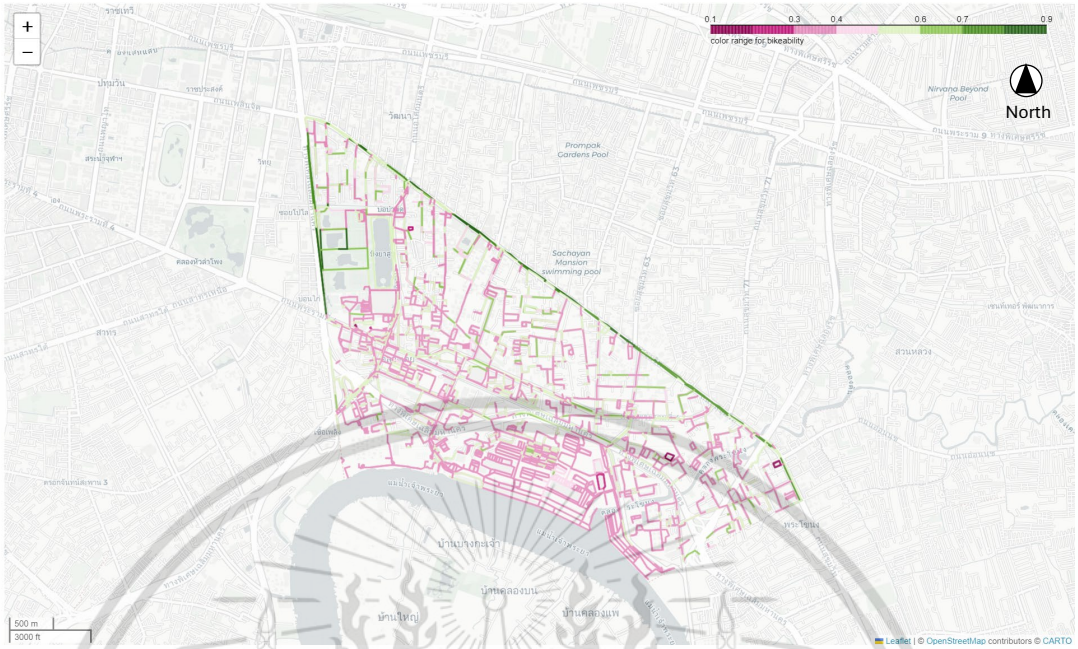

Figure 4.21 Bikeability (commuting purpose) map.

4.2.12 Recommending and Evaluating Routes

Impedance, which quantifies road weights, is the cost function to minimize when suggesting routes. Equation (14) in Chapter 3 calculates it as the ratio of the actual length of roads to their bikeability scores. A higher bikeability score results in a lower impedance score, indicating a safer, more accessible, and attractive route for cycling. To evaluate the route suggestions, this study creates 100 origin-destination (OD) pairs within a 3-kilometer Euclidean distance. We then employ the Dijkstra algorithm to identify the path with the lowest impedance score between each OD pair. We assess the recommended paths by comparing them with the shortest paths. We use difference and similarity methods for path comparison.

Out of the 100 OD pairs generated, only 98 were able to find the least-impedance path, while the remaining 2 pairs could not. Therefore, we evaluate only 98 OD pairs by comparing the least-impedance paths to the shortest paths. A high distance difference indicates significant dissimilarity. As presented in Table 4.7, the maximum distance difference is 64% longer than the shortest path. However, on average, the suggested routes provide only 5% longer distances than the shortest ones. In terms of similarity, the routes are overall 76% similar.

Table 4.7 Descriptive statistics of the metrics used in route comparison.

	count	mean	std	min	25%	50%	75%	max
shortest_length	98.0	2591.73	1090.54	307.64	1831.43	2684.93	3439.6	4985.91
impedance_length	98.0	2728.24	1200.54	366.42	1850.13	2748.44	3621.96	5620.72
intersect_length	98.0	1945.18	1091.21	0.0	1086.13	1910.88	2750.41	4139.09
distance_difference	98.0	1.05	0.1	1.0	1.0	1.01	1.05	1.64
similarity	98.0	0.76	0.29	0.0	0.65	0.88	1.0	1.0

Figure 4.22a provides an example of route comparison where the similarity hovers around the average value, showing slight differences in path selection. The least-impedance cost function generates the recommended path, represented by the red path, and the shortest path, represented by the purple path. Upon comparing the street views, it is evident that the impedance route did not select certain roads, which were populated by cars and motorcycles. Even though the street view image (shortest path) is a sample point on the road at a specific timestamp, it implies a higher potential obstacle found along the road. Higher numbers of obstacles lower the cycling suitability score since they bring discomfort and risks to bicyclists while using the roads. Figure 4.22b depicts the OD pair with approximately 60% similarity. The lower half of the routes between these two paths intersect, while the upper half clearly differs.

Figure 4.22 Comparison between the shortest (purple) and the least-impedance (red) routes

Observed street view images suggest that the selected path implies noticeably fewer obstacles on the roads, leading the algorithm to choose this route over another. Extreme scenarios where no intersection between the suggested route and the shortest route do occur. Figure 4.22c illustrates an example of a completely different route selection between the least-impedance and the shortest routes. This example shows that the least-impedance route prioritizes a route with cycleways where the impedance values are lowest which means it has the highest bikeability scores.

4.3 Discussion

We can conclude from the results obtained in this study that the recommended routes for daily use prioritize routes with bicycling infrastructure and avoid routes that have too many obstacles, such as cars, motorcycles, and pedestrians. Most people avoid routes with high accessibility because higher points of interest (POI) often result in more obstacles or crowded areas. Krenn and Titze's (2014) results guarantee the recommender's usefulness. They researched bicyclists' route choices for daily transportation and stated that bicyclists usually prefer paths with cycleways, flats, and green rather than the shortest routes. Moreover, cyclists are willing to take a longer route to avoid crowded roads (Vedel et al., 2017).

The mean distance difference between the recommended route and the shortest route is 140 meters (with a median of less than 100 meters). Thus, on average, the distance differences account for 5% longer than the shortest path. Multiple studies have investigated the actual distances bicyclists travel compared to the shortest ones for daily routines. The observed detour ratio results in a range of 7–10% (Winters et al., 2010; Titze et al., 2012; Vedel et al., 2017). Therefore, we can conclude that the recommended routes from this study provide safer and more attractive cycling routes for daily use, without any amplification of fatigue.

Chapter 5

Conclusion

5.1 Conclusion

The attempt to promote cycling as a sustainable mode of transportation in Thailand aligns with the country's ambitious goals. The country aims to achieve net-zero greenhouse gas emissions and carbon neutrality by 2050 and 2065, respectively. Challenges such as inadequate infrastructure, safety concerns, and limited cycling route planning applications remain. Overcoming these challenges necessitates a variety of approaches that support not only the expansion of cycling infrastructure, but also a focus on improving safety and the overall cycling experience. This study contributes to the advancement of sustainable urban transportation and urban planning in Thailand by leveraging data-driven methodologies and advanced technology. The goals are to create bikeability maps and safe-and-friendly cycling route recommendations tailored to Khlong Toei district, Bangkok. Even though the infrastructure for cycling won't change, the proposed framework offers a cyclist-focused approach by using bikeability scores that come from combining the three key indicators in a weighted way. Visual perception, which assesses the perceptions of the surroundings during cycling, accessibility, which reflects the availability of places and services along the route, and cycling suitability, which considers factors influencing comfort and safety for cyclists, comprise these indicators. In terms of promoting bicycle use as a daily mode of transportation, 0.31, 0.07, and 0.62 are the contributing weights for visual perception, accessibility, and cycling suitability, respectively.

We thoroughly assess the routes by comparing their distance differences and similarities to the shortest routes through the generation of 100 origin-destination (OD) pairs. The observed differences in route distances between those suggested by the proposed framework and conventional distance-based recommendations highlight the effectiveness of the proposed method in offering cyclists attractive, comfortable, and safe routes with an acceptable number of detours.

5.2 Limitation and Future Research

There are several limitations to this pilot study in Thailand. Firstly, we predominantly source the datasets from open-access platforms, which may not ensure the most up-to-date or high-quality information. OpenStreetMap (OSM) emerges as a reliable resource for road network data in cycling route recommendations due to its relatively extensive road annotation and mapping (Meng and Zheng, 2024). However, common issues include missing roads, inaccurate road tags, and disparities in data updates between urban and rural areas (Haklay and Weber, 2008). Therefore, to expand the proposed framework to other regions, we need to conduct further investigations to tackle these issues.

Secondly, the evaluation of visual perception heavily relies on data from Google Street View (GSV) images, which introduces some inaccuracies. These images, captured at different times and in different years, may not accurately reflect the real-time visual conditions encountered by cyclists. Additionally, this study used all available images, with the oldest dating back to 1970. This can lead to inaccuracies in the cyclist's perception. Therefore, future research should consider narrowing the range of image years to maintain the accuracy of the results.

Thirdly, the pre-trained segmentation model utilized for classifying street view images is trained on the Cityscapes dataset, which primarily consists of data from Germany (Cordis et al., 2016). Therefore, there may be variations in street characteristics between Thailand and the pre-trained dataset. Although the pre-trained model yields promising results for this pilot study, further refinement techniques may be necessary to tailor the segmented results to the specific characteristics of Thailand's streets.

Additionally, we may need to analyze sub-indicators like nightlight and cycleway differently. Nightlight, defined as the presence of poles in the segmented street view images, is area-specific. This means that regions with sparse nighttime lighting should still consider this indicator. However, it may be less relevant in urban areas where lights are consistently present throughout the night. Cycleways significantly influence the bikeability scores. Assigning a score of 1 to road segments that include a bikeway and a score of 0 to others results in a bimodal distribution of average indicator scores. Other road types

should receive a range of scores, rather than just one or zero, to lessen their impact on the bikeability ratings. We might adopt the variation scores from Gavalas et al. (2023).

Furthermore, this study exclusively uses open-source data. Future research should consider other indicators, such as road slopes, road surfaces, parking spots, and air pollution, which are increasingly important to the Thai public (Chulalongkorn University, 2020; Ahmed et al., 2024), if data availability remains unrestricted.

Finally, the weights integrated into this framework remain fixed to automate the selection of safer routes for daily use. However, offering users the option to customize these arbitrary weights could enhance the alignment of recommended routes with their preferences.

Drawing from the comprehensive exploration of the cycling route recommendation framework in Khlong Toei, this study sheds light on both the potential and challenges of Thailand's bikeability study. While the pilot framework demonstrates promising results in generating safer and more cyclist-friendly routes, limitations such as data quality issues, reliance on static imagery, and fixed weighting schemes underscore the need for further research and refinement. By acknowledging these limitations and advocating for user-centric customization options, future studies can strive to better align with cyclists' diverse preferences and needs. With that, they will ultimately contribute to promoting sustainable urban mobility in Thailand and beyond.

Bibliography

Achilleos, G. A. (2011). The Inverse Distance Weighted interpolation method and error propagation mechanism – creating a DEM from an analogue topographical map. *Journal of Spatial Science*, *56*(2), 283–304. https://doi.org/10.1080/14498596.2011.623348

Ahmed, T., Pirdavani, A., Wets, G., & Janssens, D. (2024). Bicycle Infrastructure Design Principles in Urban Bikeability Indices: A Systematic Review. Sustainability, 16(6), 2545. https://doi.org/10.3390/su16062545

Antón-González, L., Pans, M., José Devís-Devís, & Moreno, G. (2023). Cycling in urban environments: Quantitative text analysis. *Journal of Transport & Health*, *32*, 101651–101651. https://doi.org/10.1016/j.jth.2023.101651

Bakker, S., Guillen, M. D., Nanthachatchavankul, P., Zuidgeest, M., Pardo, C., & van Maarseveen, M. (2018). Hot or not? The role of cycling in ASEAN megacities: Case studies of Bangkok and Manila. *International Journal of Sustainable Transportation*, *12*(6), 416–431. https://doi.org/10.1080/15568318.2017.1384522

Berghoefer, F. L., & Vollrath, M. (2023). Motivational and deterrent effects of route attributes in cyclists' route choice. *Transportation Research. Part F, Traffic Psychology and Behaviour*, *95*, 343–354. https://doi.org/10.1016/j.trf.2023.04.003

Castañon, U. N., & Ribeiro, P. J. G. (2021). Bikeability and Emerging Phenomena in Cycling: Exploratory Analysis and Review. *Sustainability*, *13*(4), 2394. https://doi.org/10.3390/su13042394

Chulalongkorn University. (2020). STAY SAFE IN THE PM 2.5 Translated by Thanutra Teerasuphaset Edited by Jason Culp. https://www.chula.ac.th/wp-content/uploads/2020/01/e-Book_Stay-Safe-in-the-PM2.5-EN.pdf

Codina, O., Maciejewska, M., Nadal, J., & Marquet, O. (2022). Built environment bikeability as a predictor of cycling frequency: Lessons from Barcelona. *Transportation Research Interdisciplinary Perspectives*, *16*, 100725. https://doi.org/10.1016/j.trip.2022.100725

Bibliography (Cont.)

Cordts, M., Omran, M., Ramos, S., Rehfeld, T., Enzweiler, M., Benenson, R., Franke, U., Roth, S., & Schiele, B. (2016). *The Cityscapes Dataset for Semantic Urban Scene Understanding*. Openaccess.thecvf.com. https://openaccess.thecvf.com/content_cvpr_2016/html/Cordts_The_Cityscapes_Dataset_CVPR_2016_paper.html

Dai, S., Zhao, W., Wang, Y., Huang, X., Chen, Z., Lei, J., Stein, A., & Jia, P. (2023). Assessing spatiotemporal bikeability using multi-source geospatial big data: A case study of Xiamen, China. *International Journal of Applied Earth Observation and Geoinformation*, *125*, 103539–103539. https://doi.org/10.1016/j.jag.2023.103539

Dong, J., & Shen, G. J. (2013). A Weight-Based Road Impedance Function Model. *Advanced Materials Research*, *756-759*, 2750–2755. https://doi.org/10.4028/www.scientific.net/amr.756-759.2750

European Cyclists' Federation. (2011). *CyCle more often 2 Cool down the planet ! Quantifying Co2 savings of Cycling*. https://ecf.com/system/files/Cycle_More_Often_2_Cool_Down_the_Planet.pdf

Gavalas, D., Gerodimos, T., & Zaroliagis, C. (2023). *Context-Aware Bicycle Route Planning* (pp. 765–776). Smart Energy for Smart Transport. CSUM 2022. Lecture Notes in Intelligent Transportation and Infrastructure. Springer, Cham. https://doi.org/10.1007/978-3-031-23721-8_65

GISGeography. (2024, March 9). *Inverse Distance Weighting (IDW) Interpolation*. https://gisgeography.com/inverse-distance-weighting-idw-interpolation/Google Maps Platform. (n.d.). *Street View Image Metadata | Street View Static API*. Google Developers. https://developers.google.com/maps/documentation/streetview/metadata

Gu, P., Han, Z., Cao, Z., Chen, Y., & Jiang, Y. (2018). Using Open Source Data to Measure Street Walkability and Bikeability in China: A Case of Four Cities. *Transportation Research Record: Journal of the Transportation Research Board*, *2672*(31), 63–75. https://doi.org/10.1177/0361198118758652

Bibliography (Cont.)

Haklay, M., & Weber, P. (2008). OpenStreetMap: User-Generated Street Maps. *IEEE Pervasive Computing*, *7*(4), 12–18. https://doi.org/10.1109/MPRV.2008.80

Hallisey, K. (2022, May 11). How Riding A Bike Benefits the Environment. UCLA. https://transportation.ucla.edu/blog/how-bike-riding-benefits-environment

Hardinghaus, M., & Nieland, S. (2021). Assessing cyclists' routing preferences by analyzing extensive user setting data from a bike-routing engine. *European Transport Research Review*, *13*(1). https://doi.org/10.1186/s12544-021-00499-x

Iamtrakul, P., Chayphong, S., Kantavat, P., Hayashi, Y., Kijsirikul, B., & Iwahori, Y. (2023). Exploring the Spatial Effects of Built Environment on Quality of Life Related Transportation by Integrating GIS and Deep Learning Approaches. *Sustainability*, *15*(3), 2785. https://doi.org/10.3390/su15032785

Intergovernmental Panel on Climate Change. (2023). Synthesis report of the IPCC Sixth Assessment Report (AR6) Summary for Policymakers. In *IPCC*. Intergovernmental Panel on Climate Change. https://www.ipcc.ch/report/ar6/syr/downloads/report/IPCC_AR6_SYR_SPM.pdf

Ismain, S. H. A., Salleh, S. A., Sham, N. M., Azmi, W. N. F. W., Zulkiflee, A., & Rahman, A. Z. A. (2023). Spatial Distribution of Particulate Matter ($PM_{2.5}$) in Klang Valley using Inverse Distance Weighting Interpolation Model. *IOP Conference Series. Earth and Environmental Science*, *1217*(1), 012033–012033. https://doi.org/10.1088/1755-1315/1217/1/012033

Ito, K., & Biljecki, F. (2021). Assessing bikeability with street view imagery and computer vision. *Transportation Research Part C: Emerging Technologies*, *132*, 103371. https://doi.org/10.1016/j.trc.2021.103371

Juntakut, P., Jantakat, Y., & Shrestha, P. K. (2022). Assessing street greenery using imagery of Google Street View. *Interdisciplinary Research Review*, *17*(5), 1–5. https://ph02.tci-thaijo.org/index.php/jtir/article/view/245909

Bibliography (Cont.)

Keler, A., & Mazimpaka, J. D. (2016). Safety-aware routing for motorised tourists based on open data and VGI. *Journal of Location Based Services*, *10*(1), 64–77. https://doi.org/10.1080/17489725.2016.1170216

Kellstedt, D. K., Spengler, J. O., Foster, M., Lee, C., & Maddock, J. E. (2021). A Scoping Review of Bikeability Assessment Methods. *Journal of Community Health*, *46*(1), 211–224. https://doi.org/10.1007/s10900-020-00846-4

Krenz, K. (2017). Employing Volunteered Geographic Information in Space Syntax Analysis. *11th International Space Syntax Symposium - at Lisbon*, *11*.

Kurniawan, F., R. Arri Widyanto, & Pristi Sukmasetya. (2024). Dijkstra Algorithm Implementation to Determine the Shortest Route to Hospital: A Case Study in Magelang District Indonesia. *E3S Web of Conferences*, *500*, 01004–01004. https://doi.org/10.1051/e3sconf/202450001004

Lau, B. S. K. (2020). *Human Centric Routing Algorithm for Urban Cyclists and the Influence of Street Network Spatial Configuration*. https://repositori.uji.es/xmlui/bitstream/handle/10234/187099/Human_Centric_RA_-_blau_Braundt.pdf?sequence=1

Lee, J., Yu, K., & Kim, J. (2021). Public Bike Trip Purpose Inference Using Point-of-Interest Data. *ISPRS International Journal of Geo-Information*, *10*(5), 352. https://doi.org/10.3390/ijgi10050352

Li, J., Tian, S., Zhang, N., Liu, G., Wu, Z., & Li, W. (2023). Optimization Strategy for Electric Vehicle Routing under Traffic Impedance Guidance. *Applied Sciences*, *13*(20), 11474. https://doi.org/10.3390/app132011474

Lin, B., Saxe, S., & Timothy. (2024). AutoLTS: Automating Cycling Stress Assessment via Contrastive Learning and Spatial Post-processing. *Proceedings of the ... AAAI Conference on Artificial Intelligence*, *38*(20), 22222–22230. https://doi.org/10.1609/aaai.v38i20.30227

Lin, J.-H., & Wei, Y.-H. (2018). Assessing area-wide bikeability: A grey analytic network process. *Transportation Research Part A-Policy and Practice*, *113*, 381–396. https://doi.org/10.1016/j.tra.2018.04.022

Bibliography (Cont.)

Mamidala, R. S., Uthkota, U., Shankar, M. B., Antony, A. J., & Narasimhadhan, A. V. (2019). *Dynamic Approach for Lane Detection using Google Street View and CNN*. https://arxiv.org/pdf/1909.00798.pdf

Martin, K. (2014). *Graph Theory/Social Networks* (pp. 10–69). Spring. https://math.ou.edu/~kmartin/graphs/chap1.pdf

Meng, S., & Zheng, H. (2023). A personalized bikeability-based cycling route recommendation method with machine learning. *International Journal of Applied Earth Observation and Geoinformation*, *121*, 103373. https://doi.org/10.1016/j.jag.2023.103373

Office of Natural Resources and Environmental Policy and Planning. (2021). *Mid-century, Long-term Low Greenhouse Gas Emission Development Strategy THAILAND*. https://unfccc.int/sites/default/files/resource/Thailand_LTS1.pdf

Office of Natural Resources and Environmental Policy and Planning. (2022). *Thailand's Fourth Biennial Update Report*.

Panthasen, T., Lambregts, B., & Leopairojana, S. K. (2021). Bangkok's Bumpy Road to Sustainable Urban Mobility: Governance Challenges in the Promotion of Cycle-friendliness. *Nakhara : Journal of Environmental Design and Planning*, *20*(1), 106. https://doi.org/10.54028/nj202120106

Raha, U., & Taweesin, K. (2013). Encouraging the use of Non-motorized in Bangkok. *Procedia Environmental Sciences*, *17*, 444–451. https://doi.org/10.1016/j.proenv.2013.02.058

Ribeiro, P., Dias, G., & Mendes, G. (2022). Health-oriented routes for active mobility. *Journal of Transport & Health*, *26*, 101410–101410. https://doi.org/10.1016/j.jth.2022.101410

Rita, L., Peliteiro, M., Bostan, T.-C., Tamagusko, T., & Ferreira, A. (2023). Using Deep Learning and Google Street View Imagery to Assess and Improve Cyclist Safety in London. *Sustainability*, *15*(13), 10270. https://doi.org/10.3390/su151310270

Ritchie, H., Roser, M., & Rosado, P. (2022). Energy. *Our World in Data*. Published online at OurWorldInData.org. Retrieved from: https://ourworldindata.org/energy

Santos, B., Passos, S., Gonçalves, J., & Matias, I. (2022). Spatial Multi-Criteria Analysis for Road Segment Cycling Suitability Assessment. Sustainability, 14(16), 9928. https://doi.org/10.3390/su14169928

Bibliography (Cont.)

Schmitz, S., Zipf, A., & Neis, P. (2008). *New Applications based on collaborative geodata – the case of Routing*.

Sembiring, P., Harahap, A. S., & Zalukhu, K. S. (2018). Implementation of Dijkstra's algorithm to find an effective route to avoid traffic jam on a busy hour. *Journal of Physics: Conference Series*, *1116*(2). https://doi.org/10.1088/1742-6596/1116/2/022042

Shiode, S., & Shiode, N. (2009). New Frontiers in Urban Analysis. In Y. Asami, Y. Sadahiro, & T. Ishikawa (Eds.), *New frontiers in urban analysis* (pp. 179–196). In Honor of AtsuyukiOkabe, Chapter 10. Boca Raton.

Tanprasert, T., Siripanpornchana, C., Surasvadi, N., & Thajchayapong, S. (2020). Recognizing Traffic Black Spots From Street View Images Using Environment-Aware Image Processing and Neural Network. *Recognizing Traffic Black Spots from Street View Images Using Environment-Aware Image Processing and Neural Networ*, *8*, 121469–121478. IEEE Access. https://doi.org/10.1109/ACCESS.2020.3006493

Thitisiriwech, K., Panboonyuen, T., Kantavat, P., Iwahori, Y., & Kijsirikul, B. (2022). The Bangkok Urbanscapes Dataset for Semantic Urban Scene Understanding Using Enhanced Encoder-Decoder With Atrous Depthwise Separable A1 Convolutional Neural Networks. *IEEE Access*, *10*(56). https://doi.org/10.1109/ACCESS.2022.3176712

Tiago Tamagusko, Matheus Gomes Correia, Rita, L., Tudor-Codrin Bostan, Peliteiro, M., Martins, R., Luisa dos Santos, & Ferreira, A. (2023). Data-Driven Approach for Urban Micromobility Enhancement through Safety Mapping and Intelligent Route Planning. *Smart Cities*, *6*(4), 2035–2056. https://doi.org/10.3390/smartcities6040094

Titze, S., Krenn, P., & Oja, P. (2012). Developing a bikeability index to score the biking-friendliness of urban environments. *Journal of Science and Medicine in Sport*, *15*, S29–S30. https://doi.org/10.1016/j.jsams.2012.11.071

Tran, P. T. M., Zhao, M., Yamamoto, K., Minet, L., Nguyen, T., & Balasubramanian, R. (2020). Cyclists' personal exposure to traffic-related air pollution and its influence on bikeability. *Transportation Research Part D: Transport and Environment*, *88*, 102563. https://doi.org/10.1016/j.trd.2020.102563

Bibliography (Cont.)

Uijtdewilligen, T., Gebhard, S., Weijermars, W., Niaki, M. N., & Dijkstra, A. (2022). *Safe* https://swov.nl/en/publicatie/safe-cycling-routes.

Ungsuchaval, T., Kantamaturapoj, K., Leelahavarong, P., Yothasamut, J., Ponragdee, K., Prawjaeng, J., & Hadnorntun, P. (2022). Advocating evidence-informed policy in Thailand: The case of the development of bicycle commuting policy framework. *Case Studies on Transport Policy*, *10*(3), 1727–1734. https://doi.org/10.1016/j.cstp.2022.07.003

Vedel, S. E., Jacobsen, J. B., & Skov-Petersen, H. (2017). Bicyclists' preferences for route characteristics and crowding in Copenhagen – A choice experiment study of commuters. *Transportation Research Part A: Policy and Practice*, *100*, 53–64. https://doi.org/10.1016/j.tra.2017.04.006

Veillette, M.-P., Grisé, E., & El-Geneidy, A. (2019). Does One Bicycle Facility Type Fit All? Evaluating the Stated Usage of Different Types of Bicycle Facilities among Cyclists in Quebec City, Canada. *Transportation Research Record: Journal of the Transportation Research Board*, *2673*(6), 650–663. https://doi.org/10.1177/0361198119844741

Wage, O., & Sester, M. (2021). JOINT ESTIMATION OF ROAD ROUGHNESS FROM CROWD-SOURCED BICYCLE ACCELERATION MEASUREMENTS. *ISPRS Annals of the Photogrammetry, Remote Sensing and Spatial Information Sciences*, *V-4-2021*, 89–96. https://doi.org/10.5194/isprs-annals-v-4-2021-89-2021

Winters, M., Brauer, M., Setton, E. M., & Teschke, K. (2013). Mapping bikeability: a spatial tool to support sustainable travel. *Environment and Planning B: Planning and Design*, *40*(5), 865–883. https://doi.org/10.1068/b38185

Winters, M., Teschke, K., Grant, M., Setton, E. M., & Brauer, M. (2010). How Far Out of the Way Will We Travel? *Transportation Research Record: Journal of the Transportation Research Board*, *2190*(1), 1–10. https://doi.org/10.3141/2190-01

World Health Organization. (2018, June 17). *Global Status Report on Road Safety 2018*. World Health Organization. https://www.who.int/publications/i/item/978924156568

Bibliography (Cont.)

World Health Organization. (2022). *Cycling and walking can help reduce physical inactivity and air pollution, save lives and mitigate climate change*. Www.who.int. https://www.who.int/europe/news/item/07-06-2022-cycling-and-walking-can-help-reduce-physical-inactivity-and-air-pollution--save-lives-and-mitigate-climate-change#:~:text=walking%20for%2030%20minutes%20or

World Health Organization. (2023). *A New Year's resolution "for life."* www.who.int. https://www.who.int/thailand/news/detail/03-01-2023-a-new-year-s-resolution--for-life#:~:text=In%20its%20most%20recent%20global

Author Biography

Name	Kamonphan Phannithiprasert
Date of Birth	23 June 1998
Address	14/2 Moo.4, Rat Sathit, Chaiyo, Ang Thong 14140
Education	(2020) First Class Honors in Bachelor of Science, Geology
Scholarship	None